were passaged every 2–3 days. Embryoid bodies (EB) were derived from E14K ES cells by three-dimensional culture for 6 days in the absence of LIF. For transfection experiments, MG1.19 ES cells were cultured in the presence of 500 μg/mL G418 (Sigma) and 2 μg/mL puromycin (Sigma). Viable cell counts were performed by staining the cells with trypan blue dye and counting them on a hemocytometer. A cell-counting kit (WST-8; Dojin) was also used according to the manufacturer's protocol. Statistical analyses were performed using the paired two-tailed Student's *t* test or Welch's test using R.

Fluorescence-activated cell sorter (FACS) analysis. Single-cell suspensions of ES cells were stained with propidium iodide (PI) and analyzed using a FACSCalibur (Becton Dickinson Biosciences).

RNA isolation and RT-PCR analysis. Total RNAs were prepared with TRIzol reagent (Invitrogen), and cDNAs were prepared from total RNA using SuperScript (Invitrogen) and random primers according to the manufacturer's instructions. For PCR amplification of cDNAs, the following gene-specific primers were used:

β-actin-forward (F), CATCACTATTGGCAACGAGC;
β-actin-reverse (R), CGCAGCTCAGTAACAGTCC;
CrxOS-F (1), GTTTGAATCCTAAATCCTTAGAGC;
CrxOS-F (2), CTCCTGTACCCTGGGTCCCCTTG;
CrxOS-R, GTACCTCTTCTCCTTCCCACAAA;
ef1α-F, TCACACAGCCCACATAGCAT;
ef1α-R, CACCACTGATTAAGACTGGG;
foxD3-F, TGACCCCGAACAAGCCCAAGAACA;
foxD3-R, AGGCTCCGAAGCTCTGCATCATCA;
hprt-F, GAGATGGGAGGCCATCACATTGTG;
hprt-R, GGCCTGTATCCAACACTTCGAGAG;
nanog-F, AGGGTCTGCTACTGAGATGCTCTG;
nanog-R, CAACCACTGGTTTTTCTGCCACCG;
oct-3/4-F, CTGAGGGCCAGGCAGGAGCACGAG;
oct-3/4-R, CTGTAGGGAGGGCTTCGGGCACTT;

Preparation of anti-CrxOS antibody and Western blot analysis. A polyclonal anti-CrxOS antibody preparation (pAb) was generated by immunizing rabbits with CrxOS peptide conjugated with keyhole limpet hemocyanin and cysteine (KLH-C-QSALDGTSSPSHKA; Sigma). The anti-CrxOS pAb was used in experiments at a dilution of 1:200. For Western blots, ES cells were lysed with RIPA buffer [10 mM Tris–HCl (pH 7.4), 1 mM EDTA, 150 mM NaCl, 1% NP-40, 0.1% (w/v) sodium deoxycholate, 0.1% (w/v) SDS, 5 μg/mL aprotinin] and the supernatants were boiled with Laemmli sample buffer. Lysates were subjected to SDS–PAGE followed by immunoblotting with anti-CrxSO pAb, anti-c-Myc antibody (clone 9E10, Sigma), or anti-GAPDH antibody (clone 6C5, Santa Cruz).

Vector construction, transfection, and puromysin selection. The pPyCAGIP episomal expression vector [8] was used to make constructs containing the human histone H1 promoter and shRNA sequences as follows:

CrxOS shRNA: 5′-GATCCCCAGATTATGGTCACTAGACTGAAACTGAAATTCAAGAGATTTCAGTTTCAGTCTGGTGGCCATGATCTTTTTTGGAAA-3′; *Control* (*EGFP*) shRNA: 5′-GATCCCCGCAGCACAACTTCTCCAAGTCCACCATGCTTCAAGAGAGCATGGCGGACTTGAAGAAGTCGTGCTGCTTTTTGGAAA-3′. shRNAs were designed as described previously [9] with a slight modification. Briefly, a DNA fragment containing a Kozak sequence, a Myc tag sequence, and a multi-cloning site was inserted into EcoRI-digested pPyCAGIP to give the pPyCAGmycIP episomal expression vector [10]. For CrxOS overexpression vectors, the cDNAs encoding the long and short isoforms of CrxOS (Supplementary Fig. 1A) were obtained from E14K ES cells by PCR amplification and inserted into pPyCAGmycIP.

The RNAi-insensitive *CrxOS short* mutant was generated by introducing three silent mutations into the shRNA target sequence in *CrxOS short* such that "agatcatggcCaccagActgaaActgaaa" was converted to "agatcatggcTaccagGctgaaGctgaaa". Transfection into MG1.19 ES cells was performed with LipofectAMINE 2000 (Invitrogen) according to the manufacturer's protocol with a slight modification. Puromycin selection (2 μg/ml) was performed at 24 h post-transfection.

Results

Identification of the homeobox gene CrxOS as an ES cell-specific gene by in silico analysis

To identify ES cell-specific homeobox genes, we searched for ESTs among 240 murine genes known to contain a homeobox and registered in the NCBI EST database. We performed an *in silico* analysis of these genes by determining their levels of expression in ES cell and blastocyst cDNA libraries. We anticipated that ESTs associated with ES cell-specific homeobox genes would occur at a higher ratio in ES cells and blastocysts than would most other ESTs. After calculating EST frequencies for all 240 homeobox genes, we found that the top ten most frequent genes in ES cells and blastocysts were *CrxOS* [5], *nanog* [3], *sebox* [11], *oct3/4* [4], *gpbox* [12], Mm.158735, *pitx3* [13], Mm.201536, and *gbx-2* [14] (Supplementary Table 1). The proteins encoded by the *nanog* and *oct3/4* genes are well-known pluripotency-associated transcription factors that are crucial for stable *in vitro* propagation of ES cells in an undifferentiated state. In contrast, although *CrxOS* has been described as a homeobox gene expressed in murine retina [4], its expression and function during murine development are unknown.

CrxOS mRNA is specifically expressed in undifferentiated ES cells, blastocysts and adult testis

To examine the expression of *CrxOS* mRNA in various tissues, we performed RT-PCR and Northern analyses. *CrxOS* mRNA was expressed in undifferentiated ES cells but not in ES cells induced to differentiate by removal of LIF from the culture medium (Fig. 1A and Supplementary Fig. 1B). Furthermore, *CrxOS* mRNA

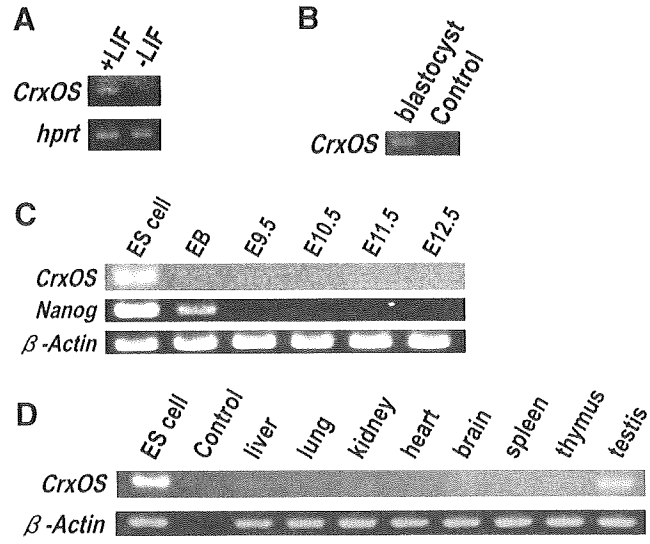

Fig. 1. Expression profiles of *CrxOS* mRNA in murine cells and tissues. (A) Dependence on LIF. E14K ES cells were cultured in the presence or absence of LIF, and levels of *CrxOS* mRNA were assessed by RT-PCR. (B, C, and D) *CrxOS* mRNA expression in mouse tissues as determined by RT-PCR. (B) Blastocysts. (C) E14K ES cells (LIF+), embryoid bodies (EB), and E9.5–E12.5 murine embryos as indicated. Nanog, positive control. β-Actin, loading control. (D) Adult murine tissues as indicated, with ES cells assessed as a positive control. Control, no reverse transcriptase.

was expressed in the blastocysts from which the ES cells had been derived (Fig. 1B), but not (unlike *nanog*) in embryoid bodies (EB) (Fig. 1C, lane 2). Neither *CrxOS* nor *nanog* mRNAs were detected in developing murine embryos at embryonic day (E) 9.5, 10.5, 11.5 or 12.5 (Fig. 1C, lanes 3–6). Interestingly, with respect to adult mouse tissues, *CrxOS* mRNA was expressed in testis but not in liver, lung, kidney, heart, brain, spleen or thymus (Fig. 1D). These results indicate that *CrxOS* mRNA expression occurs in cells and tissues linked to pluripotency, particularly undifferentiated ES cells, blastocysts and adult testis.

Dominant expression of the short isoform of CrxOS in ES cells

The *CrxOS* gene locus undergoes alternative splicing to produce two types of CrxOS isoforms: CrxOS short and CrxOS long (Fig. 2A and Supplementary Fig. 1A and B). To determine which CrxOS isoform predominated in ES cells, we used an anti-CrxOS pAb that was raised against a CrxOS peptide that is present in both isoforms (Fig. 2A). To examine endogenous CrxOS proteins, we performed Western blot analysis of ES cell extracts using anti-CrxOS pAb and detected the CrxOS short isoform but not the CrxOS long protein (Fig. 2B). Because our pAb was capable of recognizing both CrxOS proteins, this observation suggested that only the short isoform is expressed in ES cells. To further explore this hypothesis, we introduced cDNAs encoding myc-tagged CrxOS short or myc-tagged CrxOS long into MG1.19 murine ES cells, a strain in which a polyoma-based episomal vector efficiently expresses exogenous genes due to stable expression of the polyoma large T antigen [7,8]. Western blot analysis of lysates of the transfected MG1.19 ES cells using anti-myc antibody clearly revealed that the 17 kDa myc-tagged CrxOS short protein and the 30 kDa myc-tagged CrxOS long protein could be expressed in ES cells (Fig. 2C). However, when anti-CrxOS pAb was used for Western blotting of MG1.19 ES cells transfected with the expression vector for myc-tagged CrxOS short, only the endogenous and exogenous CrxOS short proteins were detected, and no endogenous CrxOS long protein (Fig. 2D, lane 2). A parallel Western analysis of MG1.19 ES cells transfected with the expression vector for myc-tagged CrxOS long exposed the presence of the endogenous CrxOS short and exogenous CrxOS long proteins (Fig. 2D, lane 3). These data indicate that

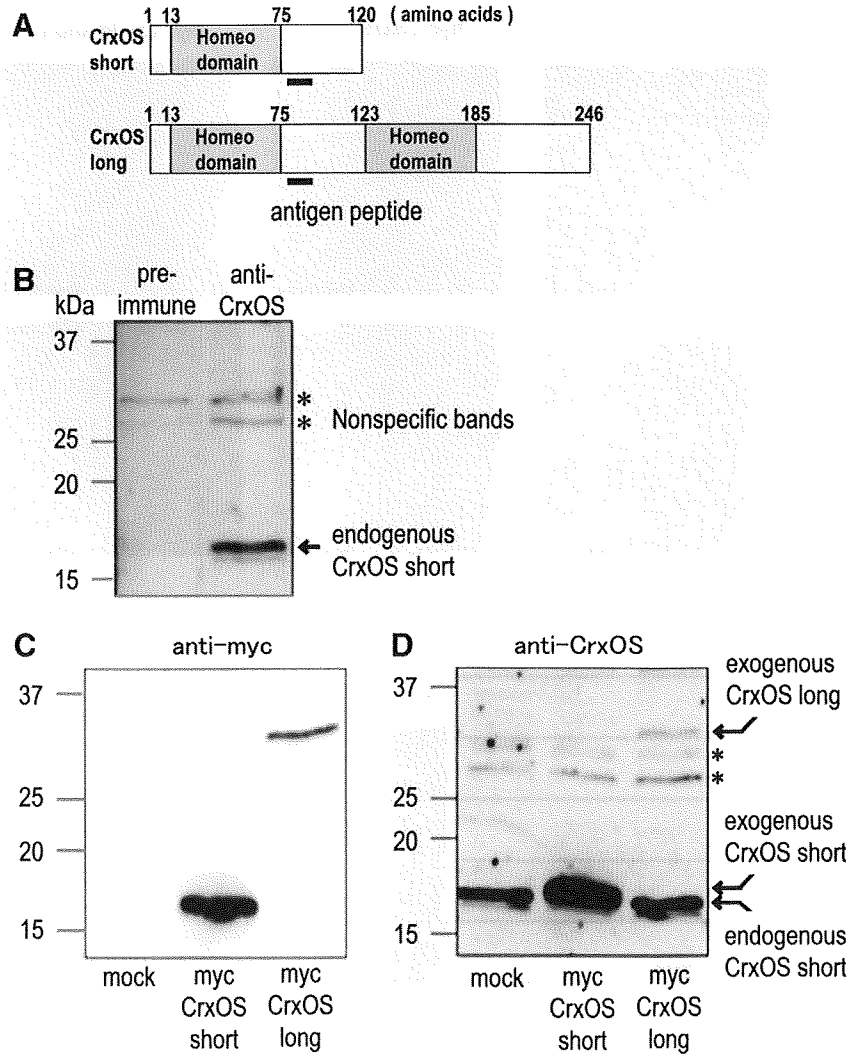

Fig. 2. Endogenous and exogenous expression of CrxOS isoforms in murine ES cells. (A) Domain structures of the CrxOS short and CrxOS long isoforms generated by alternative splicing. Black bar, synthetic peptide used as the antigen to raise anti-CrxOS pAb. (B) Expression of endogenous CrxOS short protein in MG1.19 ES cells as identified by Western blotting using anti-CrxOS pAb. Pre-immune, control antiserum. No endogenous CrxOS long protein was detected. (C) Expression of exogenous myc-tagged CrxOS short or myc-tagged CrxOS long proteins in transfected MG1.19 ES cells as detected by Western blotting using anti-myc antibody. (D) The lysates in (C) were analyzed by Western blotting using anti-CrxOS pAb. Mock, MG1.19 ES cells transfected with the parental plasmid. This plasmid does not express CrxOS proteins and the band visible in the mock-transfectants is endogenous CrxOS short protein. *non-specific bands.

the expression of the CrxOS short isoform is dominant in undifferentiated ES cells, and that our polyoma-based episomal vectors can successfully drive the expression of myc-tagged exogenous CrxOS isoforms in ES cells.

CrxOS short prevents the morphological changes triggered in ES cells by withdrawal of LIF and stimulates ES cell proliferation

In the presence of factors such as LIF, murine ES cells can maintain an undifferentiated state and undergo symmetrical self-renewal. These undifferentiated ES cells form colonies with a characteristic morphology [3,15,16] and proliferate at unusually rapid rates [17,18]. When ES cells are cultured on a monolayer without LIF, most of the cells differentiate, adopt a flattened morphology, and decrease their rate of proliferation. To examine the role of CrxOS in the differentiation and proliferation of ES cells, we took advantage of our exogenous myc-tagged *CrxOS* expression system (described in Fig. 2C and D). No significant differences in cellular morphology or numbers of viable cells were observed among control ES cells (mock-transfectants) and transfectants expressing either myc-CrxOS short or myc-CrxOS long when the cells were cultured in the presence of LIF (Fig. 3A, top panels). In the absence of LIF, control ES cells and CrxOS long-expressing transfectants both showed differentiation and a flattened morphology (Fig. 3A, bottom panels). Both these cultures also showed low numbers of viable cells (Fig. 3B). Surprisingly, colonies derived from CrxOS short-expressing transfectants were able to maintain their undifferentiated morphology and cell viability even in the absence of LIF (Fig. 3A and B). Indeed, LIF-deprived, CrxOS short-expressing transfectants proliferated just as fast as control ES cells cultured in the presence of LIF (data not shown). Thus, the short CrxOS protein prevents the differentiation of ES cells that is triggered by LIF withdrawal, and stimulates ES cell self-renewal.

CrxOS short is essential for ES cell self-renewal and prevents apoptosis

To examine the physiological function of CrxOS in ES cells, we performed *CrxOS*-knockdown experiments using RNA interference (RNAi). An shRNA construct against *CrxOS* was designed and placed under the control of the human histone H1 promoter, and this entire shRNA expression cassette was inserted into pPyCAGIP [10]. When MG1.19 ES cells were transfected with this *CrxOS* RNAi

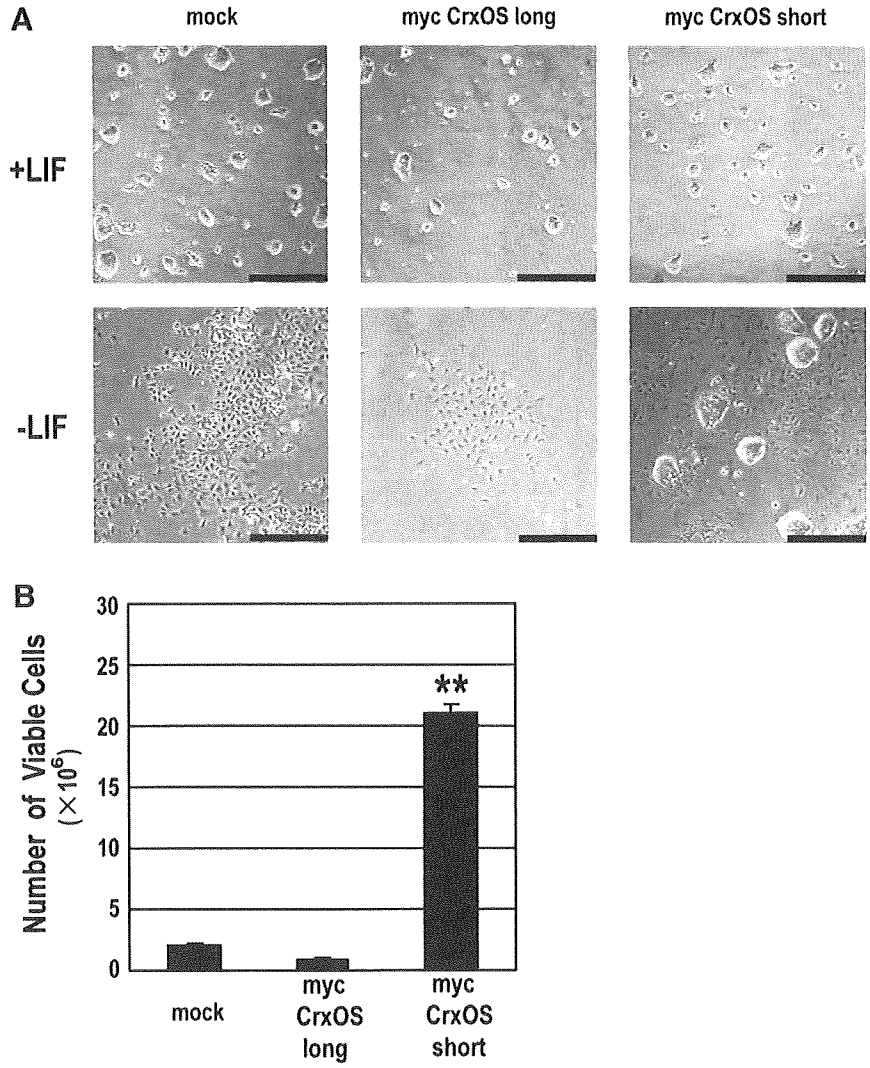

Fig. 3. Effects of overexpression of CrxOS short or long isoforms on ES cell morphology and proliferation. (A) CrxOS short maintains ES cells in an undifferentiated state. MG1.19 ES cells were transfected with the parental expression vector (mock), the myc-tagged CrxOS long expression vector, or the myc-tagged CrxOS short expression vector. Transfectants were cultured in medium containing puromycin in the presence or absence of LIF, and morphological changes were observed by phase contrast microscopy. Scale bar, 500 μm. (B) CrxOS short maintains ES cell viability. The transfectants in (A) were grown in the absence of LIF and viability was assessed by trypan blue staining. Results shown are the mean viable cell number ± s.e.m. from at least three independent experiments. $^{**}p < 0.005$.

expression vector, RT-PCR analysis showed dramatic reduction in *CrxOS* mRNA compared to cells transfected with *control* siRNA (Fig. 4A). However, we also observed a significant reduction in the number of viable cells in *CrxOS* RNAi-treated cultures compared to *control* RNAi-treated cultures in trypan blue exclusion assays (Fig. 4B). To investigate whether this drop in the number of

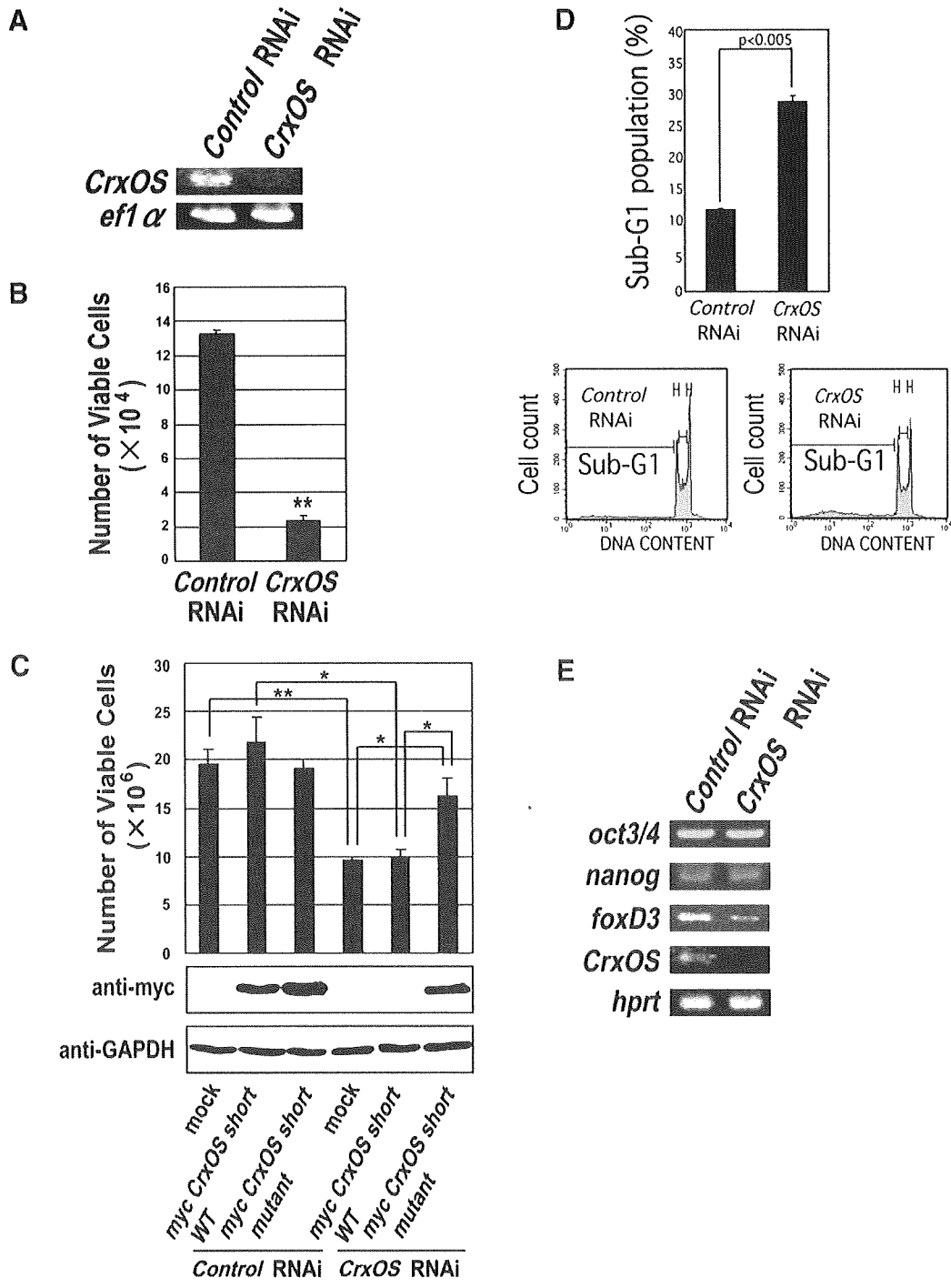

Fig. 4. CrxOS short is required for ES cell self-renewal. (A) RNAi-induced reduction of *CrxOS* mRNA. MG1.19 ES cells were transfected with *GFP* shRNA expression vector (*Control* RNAi) or *CrxOS* shRNA expression vector (*CrxOS* RNAi). Lysates were prepared and amounts of *CrxOS* mRNA were estimated by RT-PCR analysis. *ef1α*, loading control. (B) Knockdown of *CrxOS short* mRNA reduces ES cell viability. The cells in (A) were grown in the absence of LIF and stained with trypan blue. Results shown are the mean viable cell number ± s.e.m. from at least three independent experiments. $^{**}p < 0.001$. (C) Rescue of ES cell viability by ectopic overexpression of RNAi-insensitive *CrxOS short* mRNA. MG1.19 ES cells were transfected with the parental plasmid (mock), the myc-tagged *CrxOS short* expression vector (wild-type; WT), or a vector expressing a mutated form of myc-tagged *CrxOS short* that was insensitive to *CrxOS* RNAi-mediated knockdown (mutant; MT). The transfected cells were then co-transfected with the *control* RNAi or *CrxOS* shRNA expression vector. Cells were stained with trypan blue to assess viability and analyzed by Western blotting to detect levels of ectopic WT and MT CrxOS short proteins. Results shown are the mean viable cell number ± s.e.m. from at least three independent experiments. GAPDH, loading control. $^{*}p < 0.05$; $^{**}p < 0.005$. (D) Loss of CrxOS short increases ES cell apoptosis. MG1.19 ES cells were cultured in the presence of *control* RNAi or *CrxOS* RNAi, stained with PI, and analyzed by flow cytometry (lower panels). Quantitation of the subdiploid (sub-G1) peak gives the percentage of apoptotic cells (upper panel). One result representative of three experiments is shown. (E) Loss of CrxOS short decreases *foxD3* expression. The cells in (A) were analyzed by RT-PCR for mRNA levels of the indicated transcription factors known to be required for ES cell self-renewal. *hprt*, loading control.

viable cells was due to the reduction in *CrxOS short* mRNA, we performed rescue experiments using an expression vector encoding a mutant of myc-tagged CrxOS short that was insensitive to our *CrxOS* RNAi construct due to the silent mutation of three bases. In ES cells that were mock-transfected or expressed the RNAi-sensitive form of myc-tagged CrxOS short, the introduction of *CrxOS* RNAi reduced numbers of viable cells, as expected (Fig. 4C, lanes 4 and 5). However, expression of the RNAi-insensitive CrxOS short mutant allowed ES cells to resist *CrxOS* RNAi-mediated knockdown of CrxOS short and resulted in control numbers of viable cells (Fig. 4C, lane 6). These results were confirmed in experiments where cell viability was determined using the cell-counting kit, WST-8 (Supplementary Fig. 2). Thus, CrxOS expression is required for ES cell viability.

Next, we examined whether the decrease in viability of CrxOS-knockdown ES cells was due to increased apoptosis. We used flow cytometry to determine numbers of apoptotic ES cells in *CrxOS* RNAi-treated cultures and observed an increase in the sub-G1 population (apoptotic cells) in *CrxOS* RNAi-treated ES cells compared to *control* RNAi-treated cultures (Fig. 4D). Thus, CrxOS short is necessary to prevent ES cell apoptosis.

Finally, to gain mechanistic insight into how CrxOS is involved in ES cell self-renewal, we examined the mRNA expression of several transcription factors known to be required for ES cell self-renewal. No differences in the expression of *oct3/4* and *nanog* mRNAs were detected in *CrxOS* RNAi-treated ES cells but a decrease in the mRNA expression of the forkhead transcription factor FoxD3 was observed (Fig. 4E). These results suggest that the survival and proliferation of ES cells that support self-renewal are dependent on CrxOS short at least in part because CrxOS promotes *foxD3* expression.

Discussion

In this study, we have used *in silico* analyses to identify the homeobox gene *CrxOS* as an important gene expressed primarily in murine ES cells, and have shed light on CrxOS's functions in these cells using a polyoma-based episomal expression system. Firstly, we performed *in silico* gene expression analyses in ES cells and blastocysts using an NCBI EST database. Secondly, we demonstrated expression of *CrxOS* mRNA in ES cells, blastocysts and adult testis. Thirdly, we used anti-CrxOS pAb to show the dominant expression in ES cells of the CrxOS short isoform that is produced by alternative splicing. Fourthly, we demonstrated that overexpression of CrxOS short in ES cells prevents the morphological changes triggered by LIF withdrawal and stimulates ES cell proliferation. Finally, we showed that CrxOS short is required for the self-renewal of ES cells, and have provisionally identified *foxD3* as a downstream target gene of CrxOS.

The collective results of our *in silico* analyses (Supplementary Table 1) suggested that genes that are preferentially expressed in ES cells and blastocysts are critical for the pluripotency and self-renewal ability of ES cells. Our hypothesis is reinforced by the fact that *oct3/4* and *nanog*, which are known to be crucial for controlling these capacities, were among the top five genes identified in our study. Thus, our strategy for discovering genes involved in pluripotency and self-renewal in ES cells appears to be both robust and reliable.

Our examination of the homeodomain of the two CrxOS isoforms has yielded some interesting insights. CrxOS long is composed of two homeodomains: the N-terminal homeodomain and the C-terminal homeodomain, whereas CrxOS short has only the N-terminal homeodomain (Fig. 2). A phylogenetic tree generated by computer analysis revealed that none of the CrxOS homeodomains occurs in proteins belonging to the Oct3/4, Nanog or classical Hox families (Supplementary Fig. 3). Therefore, CrxOS proteins may target different DNA sequences and regulate gene expression in a manner distinct from that employed by other homeodomain proteins.

Our results suggested that CrxOS is required for *foxD3* expression in murine ES cells (Fig. 4E). The FoxD3 transcription factor is required for maintaining pluripotent cells in the early mouse embryo and for the establishment of murine ES cell lines [19,20]. FoxD3-deficient ES cells maintain a normal proliferation rate but display increased apoptosis, and clonally-dispersed FoxD3-deficient ES cells showed a decreased ability to self-renew [19,20]. Taken together with our finding that CrxOS-knockdown leads to decreased ES cell viability and increased apoptosis, we propose that at least part of CrxOS's function in ES cells is to activate *foxD3* gene expression so that self-renewal capacity is maintained. Our results thus identify CrxOS as an important regulator of self-renewal capacity in ES cells.

Acknowledgments

This work was supported in part by research grants (to H.N.) from the Ministry of Education, Culture, Sports, Science and Technology (MEXT) of Japan, and the Japan Society for the Promotion of Science (JSPS). We thank Dr. Max Gassmann for MG1.19 ES cells and the pPyCAGIP episomal expression vector. We are grateful to numerous members of the Nishina and Katada laboratories for critical reading and helpful discussions.

Appendix A. Supplementary data

Supplementary data associated with this article can be found, in the online version, at doi:10.1016/j.bbrc.2009.09.118.

References

[1] K. Kitajima, M. Masuhara, T. Era, T. Enver, T. Nakano, GATA-2 and GATA-2/ER display opposing activities in the development and differentiation of blood progenitors, EMBO J. 21 (2002) 3060–3069.
[2] S. Kanda, Y. Tamada, A. Yoshidome, I. Hayashi, T. Nishiyama, Over-expression of bHLH genes facilitate neural formation of mouse embryonic stem (ES) cells in vitro, Int. J. Dev. Neurosci. 22 (2004) 149–156.
[3] K. Mitsui, Y. Tokuzawa, H. Itoh, K. Segawa, M. Murakami, K. Takahashi, M. Maruyama, M. Maeda, S. Yamanaka, The homeoprotein nanog is required for maintenance of pluripotency in mouse epiblast and ES cells, Cell 113 (2003) 631–642.
[4] H. Niwa, J. Miyazaki, A.G. Smith, Quantitative expression of Oct-3/4 defines differentiation, dedifferentiation or self-renewal of ES cells, Nat. Genet. 24 (2000) 372–376.
[5] G. Alfano, C. Vitiello, C. Caccioppoli, T. Caramico, A. Carola, M.J. Szego, R.R. McInnes, A. Auricchio, S. Banfi, Natural antisense transcripts associated with genes involved in eye development, Hum. Mol. Genet. 14 (2005) 913–923.
[6] H. Nishina, K.D. Fischer, L. Radvanyi, A. Shahinian, R. Hakem, E.A. Rubie, A. Bernstein, T.W. Mak, J.R. Woodgett, J.M. Penninger, Stress-signaling kinase Sek1 protects thymocytes from apoptosis mediated by CD95 and CD3, Nature 385 (1997) 350–353.
[7] G. Camenisch, M. Gruber, G. Donoho, P. Van Sloun, R.H. Wenger, M.A. Gassmann, Polyoma-based episomal vector efficiently expresses exogenous genes in mouse embryonic stem cells, Nucleic Acids Res. 24 (1996) 3707–3713.
[8] M. Gassmann, G. Donoho, P. Berg, Maintenance of an extrachromosomal plasmid vector in mouse embryonic stem cells, Proc. Natl. Acad. Sci. USA 92 (1995) 1292–1296.
[9] C. Annerén, C.A. Cowan, D.A. Melton, The Src family of tyrosine kinases is important for embryonic stem cell self-renewal, J. Biol. Chem. 279 (2004) 31590–31598.
[10] J. Aubert, H. Dunstan, I. Chambers, A. Smith, Functional gene screening in embryonic stem cells implicates Wnt antagonism in neural differentiation, Nat. Biotechnol. 20 (2002) 1240–1245.
[11] M. Cinquanta, A.C. Rovescalli, A.C. Kozak, M. Nirenberg, Mouse Sebox homeobox gene expression in skin, brain, oocytes, and two-cell embryos, Proc. Natl. Acad. Sci. USA 97 (2000) 8904–8909.
[12] N. Takasaki, R. McIsaac, J. Dean, Gpbox (Psx2), a homeobox gene preferentially expressed in female germ cells at the onset of sexual dimorphism in mice, Dev. Biol. 223 (2000) 181–193.
[13] S.M. Smits, M.P. Smidt, The role of Pitx3 in survival of midbrain dopaminergic neurons, J. Neural. Transm. Suppl. 70 (2006) 57–60.
[14] A. Bulfone, L. Puelles, M.H. Porteus, M.A. Frohman, G.R. Martin, J.L. Rubenstein, Spatially restricted expression of Dlx-1, Dlx-2 (Tes-1), Gbx-2, and Wnt-3 in the

embryonic day 12.5 mouse forebrain defines potential transverse longitudinal segmental boundaries, J. Neurosci. 13 (1993) 3155–3172.
[15] I. Chambers, D. Colby, M. Robertson, J. Nichols, S. Lee, S. Tweedie, A. Smith, Functional expression cloning of Nanog, a pluripotency sustaining factor in embryonic stem cells, Cell 113 (2003) 643–655.
[16] T. Matsuda, T. Nakamura, K. Nakao, T. Arai, M. Katsuki, T. Heike, T. Yokota, STAT3 activation is sufficient to maintain an undifferentiated state of mouse embryonic stem cells, EMBO J. 18 (1999) 4261–4269.
[17] E. Stead, J. White, R. Faast, S. Conn, S. Goldstone, J. Rathjen, U. Dhingra, P. Rathjen, D. Walker, S. Dalton, Pluripotent cell division cycles are driven by ectopic Cdk2, cyclin A/E and E2F activities, Oncogene 21 (2002) 8320–8333.
[18] L. Jirmanova, M. Afanassieff, S. Gobert-Gosse, S. Markossian, P. Savatier, Differential contributions of ERK and PI3-kinase to the regulation of cyclin D1 expression and to the control of the G1/S transition in mouse embryonic stem cells, Oncogene 21 (2002) 5515–5528.
[19] L.A. Hanna, R.K. Foreman, I.A. Tarasenko, D.S. Kessler, P.A. Labosky, Requirement for Foxd3 in maintaining pluripotent cells of the early mouse embryo, Genes Dev. 16 (2002) 2650–2661.
[20] Y. Liu, P.A. Labosky, Regulation of embryonic stem cell self-renewal and pluripotency by Foxd3, Stem Cells 26 (2008) 2475–2484.

Pax6-5a Promotes Neuronal Differentiation of Murine Embryonic Stem Cells

Nao SHIMIZU,[a,b] Hajime WATANABE,[c] Junko KUBOTA,[b] Jinzhan WU,[a,b] Ryota SAITO,[a,b] Tadashi YOKOI,[a,g] Takumi ERA,[d] Takeshi IWATSUBO,[e] Takashi WATANABE,[f] Sachiko NISHINA,[g] Noriyuki AZUMA,*[,g] Toshiaki KATADA,[b] and Hiroshi NISHINA*[,a]

[a] *Department of Developmental and Regenerative Biology, Medical Research Institute, Tokyo Medical and Dental University; Tokyo 113–8510, Japan:* [b] *Department of Physiological Chemistry, Graduate School of Pharmaceutical Sciences, University of Tokyo;* [e] *Department of Neuropathology and Neuroscience, Graduate School of Pharmaceutical Sciences, University of Tokyo; Tokyo 113–0033, Japan:* [c] *Center for Integrative Bioscience, Okazaki National Research Institutes; Okazaki 444–8787, Japan:* [d] *Department of Organogenesis, Institute of Molecular Embryology and Genetics, Kumamoto University; Kumamoto 860–0811, Japan:* [f] *Department of Laboratory Medicine, Kyorin University School of Medicine; Tokyo 181–8611, Japan: and* [g] *Department of Ophthalmology, National Center for Child Health and Development; Tokyo 157–8535, Japan.* Received January 16, 2009; accepted March 11, 2009

Pax6 genes are highly conserved and important for eye development. Vertebrates predominantly produce two alternatively spliced Pax6 isoforms, Pax6 and Pax6-5a. Pax6-5a differs from Pax6 by the presence of 14 additional amino acids encoded by exon 5a. These additional amino acids occur in the Pax6 paired domain and thus influence its DNA-binding properties. However, little is known about Pax6-5a's physiological functions. Here we establish murine embryonic stem (ES) cell lines in which expression of either the human Pax6 or Pax6-5a isoform is negatively controlled by tetracycline. We report that, in contrast to Pax6 expression, Pax6-5a expression strongly induces ES cells to differentiate into neurons. Moreover, using DNA microarray analysis, we have identified the transcription factor basic helix loop–helix domain containing, class b2 (bHLHb2) in Pax6-5a-expressing ES cells. Our Pax6 isoform-expressing ES cell lines may serve as useful models for identifying Pax6-regulated genes that are important for neurogenesis and/or eye development.

Key words Pax6; Pax6-5a; embryonic stem cell; neuron; DNA microarray; basic helix loop–helix domain containing, class b2

Pax6 is a transcription factor essential for the development of the eye, brain and pancreas.[1,2] Pax6 is defined by the presence of its paired domain, a highly conserved DNA-binding motif composed of two distinct DNA-binding subdomains called the N-terminal subdomain (NTS) and the C-terminal subdomain (CTS). The NTS and the CTS bind to distinct consensus DNA sequences.[3,4] Transcription of the human *Pax6* gene results in two alternatively spliced isoforms, Pax6 and Pax6-5a. Compared to Pax6 transcripts, Pax6-5a transcripts contain an additional exon 5a that encodes an additional 14 amino acids. These amino acids are inserted into the NTS, an event that abolishes the DNA-binding activity of this subdomain and unmasks the DNA-binding activity of the CTS. Thus, exon 5a transcription appears to function as a molecular switch that regulates the spectrum of Pax6 target genes that can be induced. Previously, we reported a missense mutation in the exon 5a region of the *Pax6* gene in patients with Peters anomaly. This mutation resulted in a Pax6 protein with impaired DNA-binding and transactivation activities.[5] Subsequently, we found that although overexpression of either Pax6 or Pax6-5a in chick embryos induced transdifferentiation of ectopic neural retina from primitive retinal pigment epithelium, Pax6-5a was a much stronger driver of this process than was Pax6.[6,7] However, little is known about how Pax6 and Pax6-5a actually function *in vivo*.

Embryonic stem (ES) cells are pluripotent cells derived from the inner cell mass of preimplantation mouse embryos. ES cells can be propagated stably in the undifferentiated state *in vitro* and, under the appropriate culture conditions, can be induced to differentiate into a variety of cell types. For example, forced transgenic expression of Pdx1 causes ES cells to differentiate into pancreatic cells (endoderm), whereas GATA2 expression promotes leukocyte differentiation (mesoderm), and Mash1 expression induces neuronal differentiation (ectoderm).[8,9] This plasticity makes ES cell culture a useful tool for elucidating the functions of transcription factors.

In this report, we have employed conditional expression of human Pax6-5a driven by a tetracycline-regulatable promoter and have found that forced Pax6-5a expression in murine ES cells enhances their differentiation into neuronal cells. Our system may be useful for uncovering the molecular mechanisms underlying Pax6-5a-dependent eye development.

MATERIALS AND METHODS

Establishment of Tet-Regulated ES Cell Clones The murine ES cell line E14tg2a was maintained in Dulbecco's modified Eagle's medium (DMEM) supplemented with 15% fetal calf serum, 0.1% β-mercaptoethanol, and 1000 U/ml leukemia inhibitory factor (LIF). The tetracycline (Tet) regulatory system was used to obtain inducible Pax6- or Pax6-5a-expressing ES cell clones as described previously.[10] Briefly, Tet-regulatable Flag-Pax6 and Flag-Pax6-5a constructs were generated by inserting Flag-human Pax6 or Flag-human Pax6-5a cDNA into the NotI site of pUHD10-3.IRES-EGFP. Expression of these Tet-regulatable constructs in ES cells was completely suppressed by the addition of tetracycline to the culture medium. The ES cell clones whose enhanced green fluorescent protein (EGFP) expression was most tightly regulated by tetracycline were selected for further study, including examination of the expression of relevant genes by reverse transcription-polymerase chain reaction

* To whom correspondence should be addressed. e-mail: nishina.dbio@mri.tmd.ac.jp; azuma-n@ncchd.go.jp

(RT-PCR) and Western blotting.

ES Cell Differentiation Embryoid bodies (EBs) were prepared as described previously.[11] Briefly, undifferentiated ES cells were dissociated into single-cell suspensions and cultured in hanging drops to induce embryoid body (EB) formation. Initial cell density was 2000 cells per drop (25 μl) of differentiation medium without LIF in the absence or presence of 1 μg/ml Tet (Day 0). After 2 days in a hanging drop culture (Day 2), the resulting EBs were transferred to non-coated culture dishes. On Day 3, bFGF (20 ng/ml, R&D Systems) was added to the culture medium. On Day 7, the EBs were plated in plastic gelatin-coated dishes.

Immunoprecipitation and Immunoblotting For detection of induced Flag-Pax6 and Flag-Pax6-5a proteins, ES cells were cultured for 48 h in the absence of Tet. ES cells (5×10^6) were then lysed and immunoprecipitated with anti-Flag M2 antibody (Ab) (Sigma, F3165). The immunoprecipitates were fractionated by sodium dodecyl sulfate-polyacrylamide gel electrophoresis (SDS-PAGE) and immunoblotted with anti-Flag M2 Ab. Bands were visualized using the SuperSignal West Pico chemiluminescent substrate according to the manufacturer's instructions (PIERCE, IL, U.S.A.).

Confocal Microscopy Immunofluorescence studies were performed as described previously.[12] Briefly, EBs cultured on gelatin-coated dishes were washed three times with phosphate buffered saline (PBS) and fixed in 4% paraformaldehyde. After permeabilization with 0.2% Triton X-100, the EBs were incubated with blocking solution [5% bovine serum albumin (BSA) in TBS], followed by anti-βIII-tubulin Ab (Covance, MMS-435P). The stained EBs were washed with PBS and incubated with Alexa-568-conjugated secondary Ab (Molecular Probes). After a last wash in PBS, EBs were viewed on a Carl Zeiss confocal microscope equipped with LSM510 software.

RT-PCR Analysis ES cells were lysed with Trizol reagent (Invitrogen) and first-strand cDNA was synthesized by using SuperScript III RNase H-reverse transcriptase (Invitrogen). Primers used were: Flag-Pax6, 5′-ATGGATTACAAGGATGACGACG-3′ and 5′-ATCTGTTGCTTTTCGCTAGCC-3′; Acetylcholine esterase (Ache), 5′-CCGATTTTCCTTCGTGCCTG-3′ and 5′-TGGAGGCACGGTGTTCAAAG-3′; Serotonin receptor 5a (5-HT5a), 5′-AGTCGGCCTTTTCTCTCAGC-3′ and 5′-GGTCCAGTGCTATTGCTGTC-3′; L1, 5′-AGGACACCATGTGCTAGAGC-3′ and 5′-GGGTTGCAAGGCAGAACTAC-3′; Elongation factor 1 (EF1), 5′-TCACACAGCCCACATAGCAT-3′ and 5′-CACCACTGATTAAGACTGGG-3′; Oct3/4, 5′-CTGAGGGCCAGGCAGGAGCACGAG-3′ and 5′-CTGTAGGGAGGGCTTCGGGCACTT-3′; bHLHb2, 5′-TTATTGCACAGCTAGACACGG-3′ and 5′-ACACTGTAACCTCGCCTCTC-3′.

DNA Microarray Total RNAs from EBs were extracted using TRIZOL (Invitrogen, Tokyo, Japan) and purified using an RNeasy mini kit (Qiagen, Tokyo, Japan). Purified RNA was labeled with biotin according to the manufacturer's protocol and hybridized to a mouse genome 430A 2.0 array (Affymetrix Japan, Tokyo, Japan). After washing, the array was scanned to measure fluorescence intensity (representing gene expression). The fluorescence intensity of each probe was further analyzed by dChip, a model-based expression analysis program that estimates gene expression levels. For the dChip analysis, a perfect match (PM)-only model was used. The estimated gene expression level values were applied to the Gene-Spring software program (Silicon Genetics, Redwood City, CA, U.S.A.).[13]

Construction of Plasmids A DNA fragment encompassing −90 to −1996 bp of the 5′ region of the murine *bHLHb2* gene was subjected to PCR amplification using the iProof High Fidelity DNA Polymerase system (BioRad). After digestion with *Mlu*I and *Xho*I, the PCR product was subcloned into the *Mlu*I/*Xho*I sites of the pTA-Luc vector (CLONTECH), resulting in pbHLHb2 (−90—−1996). To construct the pTA-5aCON-Luc vector, which served as a positive control for the Pax6-5a reporter assay, the oligonucleotides 5′-AAATCTGAACATGCTCAGTGAATGTTCATTGACTCTCGAGGTC-3′ and 5′-GACCTCGAGAGTCAATGAACATTCACTGAGCATGTTCAGATTT-3′ were annealed, phosphorylated and ligated into the *Sma*I site of the pTA-Luc vector. Underlining indicates Pax6-5a binding sequences.

Transient DNA Transfections and Luciferase Reporter Assays DNA transfections were carried out using the Lipofectamine 2000 reagent (Invitrogen). Briefly, the human embryonic carcinoma cell line NTERA2 were plated in a 24-well plate. After 24 h transfection with the above reporter plasmids, the cells were harvested and firefly and sea pansy luciferase activities were determined using the dual-luciferase reporter assay system (Promega) and a Wallac ARVO.SX 1420 Multilabel Counter (Amersham Pharmacia Biotech). All experiments were repeated at least three times with different batches of transfected cells and the results were fully reproducible.

RESULTS

Tet-regulatable Pax6 and Pax6-5a Expression To investigate the biological functions of Pax6 and Pax6-5a, we established murine ES cell lines with tetracycline (Tet)-regulatable Flag-human Pax6 or Flag-human Pax6-5a expression. To this end, a Tet-regulatable bicistronic vector encoding Flag-Pax6 or Flag-Pax6-5a plus the EGFP was introduced into ES cells. ES cell lines were then established in the presence of Tet (Tet-on) to suppress the expression of the exogenous Flag-Pax6 or Flag-Pax6-5a. Conditional expression of Flag-Pax6 or Flag-Pax6-5a and EGFP in these ES cells was achieved by withdrawal of Tet (Tet-off). The successful expression of Flag-Pax6 and Flag-Pax6-5a proteins in Tet-off ES cell lines was confirmed by Western blot analysis using anti-Flag antibody (Fig. 1A), whereas EGFP expression was detected with confocal microscopy (Fig. 1B). These results confirm that our Pax6 isoform-expressing ES cell lines showed EGFP plus exogenous Pax6 or Pax6-5a protein expression that was fully regulated by Tet.

Pax6-5a Expression Enhances Neuronal Differentiation by ES Cells Cultured murine ES cells can be induced to differentiate *in vitro* into a variety of cell types, including cardiac cells and neurons. To separately examine the effects of Pax6 and Pax6-5a on ES cell differentiation, we cultured our Tet-regulatable ES cell lines without LIF in the presence or absence of Tet and allowed them to form embryoid bodies (EBs). Interestingly, Tet-regulatable Pax6-5a-expressing ES cells differentiated into neuron-like cells in absence, but not presence, of Tet (Fig. 2A). To confirm that the observed dif-

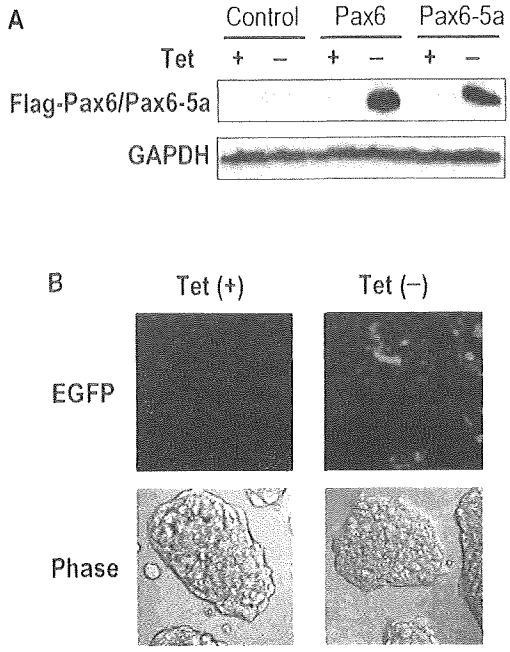

Fig. 1. Establishment of Murine ES Cell Lines with Tet-Regulatable Expression of Pax6 Isoforms

(A) Confirmation of Tet-regulated expression by Western blot. Murine ES cell lines expressing either EGFP vector alone (control) or EGFP plus either Flag-human Pax6 (Pax6) or Flag-human Pax6-5a (Pax6-5a) were cultured with (+) or without (−) Tet for 2 d and subjected to Western blotting using anti-Flag Ab. GADPH, loading control. (B) Confirmation of transfection. Detection of EGFP expression in monolayers of Tet-regulatable Pax6-5a-expressing ES cells in the presence or absence of Tet. Top, confocal microscopy; bottom, phase contrast microscopy. For all figures, results shown are one trial representative of at least three independent experiments.

ferentiating cells were in fact neurons, we immunostained them with anti-βIII-tubulin Ab and obtained positive results (Fig. 2A, right panel). On the other hand, this type of neuronal differentiation did not occur in Tet-off Pax6-expressing ES cells (data not shown). We then used RT-PCR to examine the expression by both of our Tet-regulatable ES cell lines of typical neuronal marker genes such as acetylcholinesterase (Ache; cholinergic neurons), serotonin receptor 5a (5-HT5a; serotonergic neurons), and L1 (neuronal cell adhesion molecule). Expression levels of Ache, 5-HT5a and L1 mRNAs were increased in Tet-off Pax6-5a-expressing ES cells, but not in Tet-on Pax6-5a-expressing ES cells, nor in Tet-off or Tet-on Pax6-expressing ES cells (Fig. 2B). These data indicate that expression of Pax6-5a by murine ES cells enhances their neuronal differentiation.

Pax6-5a Expression Enhances Neurite Development by Murine EBs To determine the timing of Pax6-5a-induced neuronal commitment, we examined neurite development in EB cultures of Pax6-5a-expressing ES cells from which Tet was removed for 0, 1, 2, 3, 4 or 11 d after Day 0 (Fig. 3A). When Tet was withdrawn for 11 d, more than 60% of EBs were found to be neurite-positive (Fig. 3B, row f). The most dramatic increase in the percentage of neurite-positive EBs observed occurred between 2 d (condition c) and 3 d (condition d) of Tet withdrawal, suggesting that Pax6-5a-induced neuronal commitment is established in this system during the first 3 d of culture.

Pax6-5a Expression Upregulates Neuron-Related Genes in Murine EBs To determine the identity of genes activated downstream of Pax6-5a, we performed a DNA mi-

Fig. 2. Pax6-5a Enhances the Neuronal Differentiation of Murine ES Cells

(A) Neuron-like differentiation. Tet-regulatable Pax6-5a-expressing ES cells were allowed to form EBs in the presence or absence of Tet, followed by immunostaining with anti-βIII-tubulin Ab. (B) Neuronal marker expression. Control, Pax6- and Pax6-5a-expressing ES cell lines were cultured in the presence or absence of Tet for 11 d and expression levels of the neuronal marker genes Ache, 5-HT5a and L1 were determined by RT-PCR. EF1, loading control.

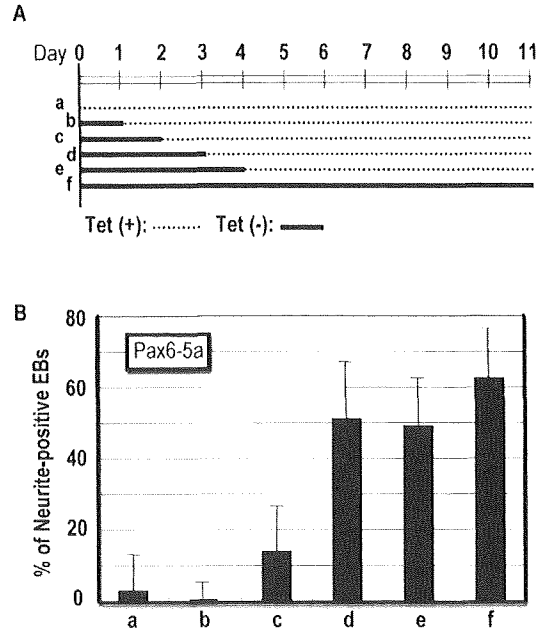

Fig. 3. Time Course of Pax6-5a-Induced Commitment to ES Cell Neuronal Differentiation

(A) Experimental scheme. Tet-regulatable Pax6-5a-expressing ES cells were cultured with Tet for 0—11 d as indicated (a—f). EB formation commenced on Day 0 and neuronal differentiation was assessed on Day 11. (B) Day 3 commitment. Percentages of neurite-positive EBs in the cultures in (A) were assessed by microscopy. A significant increase in neurite-positive EBs occurs between Day 2 and Day 3.

croarray analysis of Tet-regulatable Pax6-5a ES cells cultured for 3 d in the absence or presence of Tet. Among the many genes whose expression was increased in a Pax6-5a-dependent manner were the transcription factors basic helix-loop–helix domain containing, class b2 (bHLHb2) and Oct3/4 (data not shown). Both bHLHb2 and Oct3/4 are able to induce ES cells to differentiate into neuronal cells.[14,15] To confirm the effects of Pax6-5a on the expression of bHLHb2 and Oct3/4, we carried out an RT-PCR time course analysis of Tet-regulatable Pax6- or Pax6-5a-expressing ES cells cultured in the presence or absence of Tet for 1—5 d. bHLHb2 mRNA expression was constant in Tet-on and Tet-off Pax6-expressing ES cells regardless of the number of days of Tet withdrawal, whereas Oct3/4 expression declined in a time-dependent manner in both Tet-on and Tet-off Pax6-expressing ES cells (Fig. 4A, upper panel). In contrast, expression levels of both bHLHb2 and Oct3/4 mRNAs were increased in Tet-off Pax6-5a-expressing ES cells compared to Tet-on Pax6-5a-expressing ES cells (Fig. 4A, lower panel). These results suggest that *bHLHb2* and *Oct3/4* are downstream target genes of Pax6-5a.

To determine whether the *bHLHb2* gene was truly a transcriptional target of Pax6-5a, we carried out luciferase reporter assays examining *bHLHb2* promoter activity. A DNA fragment encompassing −90 to −1996 bp of the 5′ region of the murine *bHLHb2* gene was positioned upstream of the pTA-Luc firefly luciferase reporter gene to create the pTA-bHLHb2-Luc reporter. This reporter was cotransfected along with a plasmid expressing Pax6-5a into NTERA2 cells, a human embryonic carcinoma cell line. As a positive control, we generated the pTA-5aCON-Luc reporter plasmid that contains a Pax6-5a-binding sequence and responds to Pax6-5a. Interestingly, the degree of induction of pTA-bHLHb2-Luc was equivalent to that of pTA-5aCON-Luc, indicating that the *bHLHb2* gene is directly or indirectly regulated by Pax6-5a at least in NTERA2 cells.

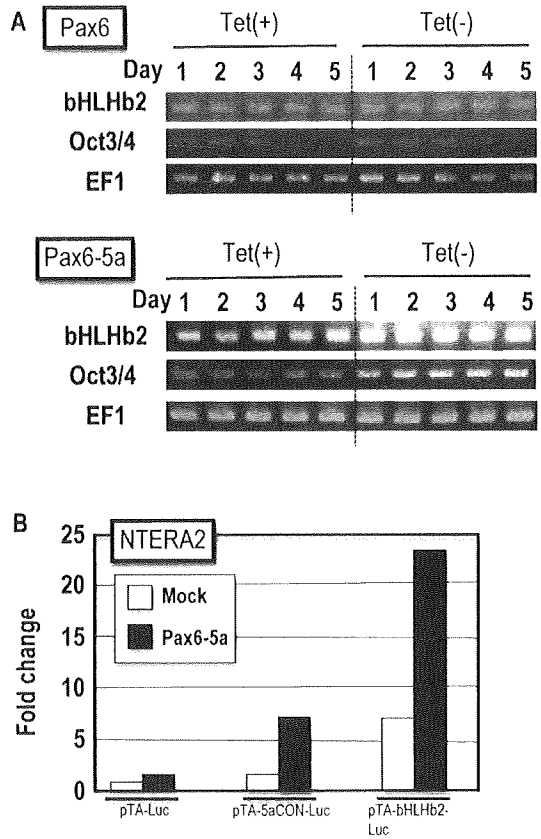

Fig. 4. Influence of Pax6-5a on *bHLHb2* and *Oct3/4* Gene Expression and *bHLHb2* Transcriptional Activity

(A) Increased *bHLHb2* and *Oct3/4* expression. Tet-regulatable Pax6- or Pax6-5a-expressing ES cells were cultured for the indicated times in the presence or absence of Tet and levels of bHLHb2 and Oct3/4 mRNAs were assessed by RT-PCR. (B) *bHLHb2* is a Pax6-5a target gene. NTERA2 cells were co-transfected with a plasmid expressing Pax6-5a or the vehicle alone (mock), plus the indicated luciferase reporter constructs: pTA-Luc (negative control), pTA-5aCON-Luc (positive control) or pTA-bHLHb2-Luc (5′ region of the *bHLHb2* gene). Results shown are the fold change in luciferase activity relative to negative control.

DISCUSSION

In this study, we have shed light on the function of the Pax6-5a isoform using a Tet-regulated conditional expression system in the context of EB-mediated ES cell differentiation into neuronal cells. Firstly, we established ES cell lines in which the expression of human Pax6 or Pax6-5a was regulated by the presence or absence of Tet. Secondly, we demonstrated that expression of Pax6-5a, but not Pax6, enhanced the differentiation of EBs, but not monolayer ES cells, into Ache$^+$ 5-HT5a$^+$ L1$^+$ neuron-like cells. Thirdly, we showed that Pax6-5a-induced neuronal commitment occurs within the first 3 d of EB formation. Finally, we provisionally identified *bHLHb2* and *Oct3/4* as downstream target genes of Pax6-5a.

We have previously described a missense mutation within *Pax6* exon 5a in four families with members suffering from Peters anomaly, congenital cataracts, Axenfeldt anomaly, and/or foveal hypoplasia.[5] Biochemical analysis showed that this mutation caused a decrease in CTS transactivation activity. Singh *et al.* have reported iris hypoplasia and defects in the cornea, lens and retina in mice lacking *Pax6* exon 5a.[16] On the other hand, overexpression of Pax6-5a induces a remarkably well-differentiated retina-like structure in chick embryos.[6] The collective results of these "loss of function" and "gain of function" studies suggest that the evolution of the Pax6-5a isoform has contributed to the advanced features of the vertebrate eye. Our data are consistent with this hypothesis, in that forced expression of Pax6-5a, but not Pax6, strongly induced the neuronal differentiation of ES cells.

As shown in Fig. 1, our established ES cell lines showed EGFP plus exogenous Pax6 or Pax6-5a protein expression that was strictly regulated by Tet in monolayer-culture conditions. However, the percentage of neuronal differentiation from EB culture, which is a kind of three-dimensional culture, were 23% in the presence of Tet and 97% in the absence of Tet, respectively (data not shown). We could observe the expression of neuronal marker genes such as L1 and Ache even in the presence of Tet by RT-PCR (Fig. 2B). We speculate that Tet is less effective for EB culture compared to monolayer culture, resulting in a leak of Pax6-5a expression and an induction of neuronal differentiation from EB culture.

As mentioned above, the paired domain of Pax6 is composed of two subdomains: NTS (also called PAI) and CTS (also called RED). Each subdomain recognizes a distinct half-site of the bipartite Pax6 binding site positioned in adjacent major grooves of the DNA. In Pax6-5a, the NTS domain is modified by the insertion of 14 amino acids encoded by

the additional exon 5a. This addition alters the DNA-binding specificity of the paired domain such that it recognizes a new consensus sequence, 5aCON. The 5aCON sequence consists of four interdigitated 5′ half-sites of the bipartite consensus sequence and is thus bound by four Pax6-5a molecules *via* the intact CTS domain. A previous study of transgenic mice overexpressing human Pax6-5a in the lens showed that the human α5 and β1 integrin promoters contain both Pax6 and Pax6-5a binding sites and maybe directly regulated by Pax6 isoforms.[17] Another report based on a genome database search and biochemical analysis showed that an enhancer present in the γE- and γF-crystallin genes is recognized by both Pax6 and Pax6-5a.[18] However, there is little physiological data on genes that are regulated by Pax6-5a, either directly or indirectly. Therefore, our Tet-regulatable Pax6 isoform-expressing ES cell lines should be useful for identifying target genes of Pax6 and/or Pax6-5a. Indeed, we found that expression levels of Oct3/4 and hHLHb2 were strikingly influenced by Pax6-5a.

In vivo, Oct3/4 plays a critical role in maintaining ES cell pluripotency. *In vitro*, sustained transgenic Oct3/4 expression in ES cells cultured in serum-free LIF-deficient medium causes accelerated differentiation to neuroectoderm-like cells, whereas suppression of Oct3/4 abolishes neuronal differentiation.[15] Thus, Oct3/4 promotes neuroectoderm formation and subsequent ES cell differentiation into neuronal cells. Our data indicate that the activation of Oct3/4 necessary for neuroectoderm formation depends on Pax6-5a activity. The other gene we found to be regulated by Pax6-5a, *bHLHb2*, encodes a basic helix–loop–helix protein with significant sequence similarities to the *Drosophila* hairy and enhancer-of-split proteins as well as mouse Hes proteins. Overexpression of bHLHb2 in monolayers of P19 embryonal carcinoma cells results in neuronal differentiation under conditions where P19 cells typically undergo only mesodermal/endodermal differentiation.[14] Thus, bHLHb2 is thought to be a repressor of several of the cell fate decisions that occur during cellular differentiation. Our data indicate that Pax6-5a may regulate bHLHb2 activation and thus determine neuronal differentiation during embryogenesis. With respect to adult vertebrates, Pax6 has been shown to be required for the production and maintenance of progenitor cells during postnatal hippocampal neurogenesis.[19] Thus, Pax6 plays important roles in both embryogenesis and adult body homeostasis. Our results suggest that Pax6-5a may be the Pax6 isoform most critical for influencing the neuronal differentiation necessary for these processes.

Acknowledgments This work was supported in part by research grants (to H.N.) from the Ministry of Education, Culture, Sports, Science and Technology (MEXT) of Japan, and the Japan Society for the Promotion of Science (JSPS). We are grateful to numerous members of the Nishina and Katada laboratories for critical reading and helpful discussions.

REFERENCES

1) Gehring W. J., *Int. J. Dev. Biol.*, **46**, 65—73 (2002).
2) Pichaud F., Desplan C., *Curr. Opin. Genet. Dev.*, **12**, 430—434 (2002).
3) Epstein J. A., Cai J., Glaser T., Jepeal L., Maas R. L., *J. Biol. Chem.*, **269**, 8355—8361 (1994).
4) Epstein J. A., Glaser T., Cai J., Jepeal L., Walton D. S., Maas R. L., *Genes Dev.*, **8**, 2022—2034 (1994).
5) Azuma N., Yamaguchi Y., Handa H., Hayakawa M., Kanai A., Yamada M., *Am. J. Hum. Genet.*, **65**, 656—663 (1999).
6) Azuma N., Tadokoro K., Asaka A., Yamada M., Yamaguchi Y., Handa H., Matsushima S., Watanabe T., Kohsaka S., Kida Y., Shiraishi T., Ogura T., Shimamura K., Nakafuku M., *Hum. Mol. Genet.*, **14**, 735—745 (2005).
7) Azuma N., Tadokoro K., Asaka A., Yamada M., Yamaguchi Y., Handa H., Matsushima S., Watanabe T., Kida Y., Ogura T., Torii M., Shimamura K., Nakafuku M., *Hum. Mol. Genet.*, **14**, 1059—1068 (2005).
8) Kitajima K., Masuhara M., Era T., Enver T., Nakano T., *EMBO J.*, **21**, 3060—3069 (2002).
9) Kanda S., Tamada Y., Yoshidome A., Hayashi I., Nishiyama T., *Int. J. Dev. Neurosci.*, **22**, 149—156 (2004).
10) Era T., Witte O. N., *Proc. Natl. Acad. Sci. U.S.A.*, **97**, 1737—1742 (2000).
11) Takayanagi H., Kim S., Koga T., Nishina H., Isshiki M., Yoshida H., Saiura A., Isobe M., Yokochi T., Inoue J., Wagner E. F., Mak T. W., Kodama T., Taniguchi T., *Dev. Cell*, **3**, 889—901 (2002).
12) Kitagawa D., Kajiho H., Negishi T., Ura S., Watanabe T., Wada T., Ichijo H., Katada T., Nishina H., *EMBO J.*, **25**, 3286—3297 (2006).
13) Watanabe H., Suzuki A., Kobayashi M., Takahashi E., Itamoto M., Lubahn D.B., Handa H., Iguchi T., *J. Mol. Endocrinol.*, **30**, 347—358 (2003).
14) Boudjelal M., Taneja R., Matsubara S., Bouillet P., Dolle P., Chambon P., *Genes Dev.*, **11**, 2052—2065 (1997).
15) Shimozaki K., Nakashima K., Niwa H., Taga T., *Development*, **130**, 2505—2512 (2003).
16) Singh S., Mishra R., Arango N. A., Deng J. M., Behringer R. R., Saunders G. F., *Proc. Natl. Acad. Sci. U.S.A.*, **99**, 6812—6815 (2002).
17) Duncan M. K., Kozmik Z., Cveklova K., Piatigorsky J., Cvekl A., *J. Cell Sci.*, **113**, 3173—3185 (2000).
18) Kralova J., Czerny T., Spanielova H., Ratajova V., Kozmik Z., *Gene*, **286**, 271—282 (2002).
19) Maekawa M., Takashima N., Arai Y., Nomura T., Inokuchi K., Yuasa S., Osumi N., *Genes Cells*, **10**, 1001—1014 (2005).

J Gastroenterol
DOI 10.1007/s00535-009-0042-x

ORIGINAL ARTICLE—LIVER, PANCREAS, AND BILIARY TRACT

Down-regulation of hepatic stearoyl-CoA desaturase 1 expression by angiotensin II receptor blocker in the obese *fa/fa* Zucker rat: possible role in amelioration of insulin resistance and hepatic steatosis

Junji Yokozawa · Takashi Sasaki · Kumiko Ohwada · Yayoi Sasaki · Jun-Itsu Ito · Takafumi Saito · Sumio Kawata

Received: 30 June 2008 / Accepted: 5 January 2009

Abstract
Background It has been reported that angiotensin II type 1 receptor blocker (ARB) can ameliorate hepatic steatosis and insulin resistance. Stearoyl-CoA desaturase 1 (SCD-1), which catalyzes the cellular synthesis of monounsaturated fatty acids, affects lipid metabolism. In this study, we investigated whether SCD-1 gene expression is affected by ARB treatment.
Methods Obese *fa/fa* Zucker rats fed a high-fat diet were treated with a potent ARB and olmesartan, and the resulting changes in the components of serum and liver were studied. Gene expression of hepatic SCD-1 was assayed using real-time PCR.
Results The serum glucose and insulin levels and hepatic TG content of the obese Zucker rats fed a high-fat diet were reduced after olmesartan administration, while the serum adiponectin level was increased. Real-time PCR revealed an increase of SCD-1 gene expression in the liver of these rats, followed by a reduction after olmesartan administration. The ratio of stearic acid (C18:0) to oleic acid (C18:1) in the liver was increased by olmesartan, indicating a reduction in the in vivo activity of SCD-1.
Conclusions ARB ameliorates hepatic steatosis and insulin resistance in obese *fa/fa* Zucker rats fed a high-fat diet. Gene expression of SCD-1 is decreased by olmesartan, suggesting that the beneficial effect is due partly to suppression of the key enzyme for hepatic lipid metabolism by ARB.

J. Yokozawa · T. Sasaki · K. Ohwada · Y. Sasaki · J.-I. Ito · T. Saito · S. Kawata (✉)
Department of Gastroenterology, Faculty of Medicine, Yamagata University, 2-2-2 Iida-Nishi, Yamagata 990-9585, Japan
e-mail: kawata@med.id.yamagata-u.ac.jp

Keywords Hepatic steatosis · Insulin resistance · Stearoyl-CoA desaturase 1 · Adiponectin · Angiotensin II type 1 receptor blocker

Introduction

Metabolic syndrome is a cluster of metabolic alterations whose landmarks include visceral obesity, hyperlipidemia, hepatic steatosis, and insulin resistance [1]. A diet with a high carbohydrate and fat content is considered to be a causative factor in the development of insulin resistance in animals and humans [2–6].

Several lines of evidence have suggested that the renin–angiotensin system (RAS) participates in insulin resistance. Adipocytes are known to secrete angiotensinogen and angiotensin II (Ang II) as adipocytokines [7, 8]. Ang II induces insulin resistance via suppression of intracellular signal transduction of insulin and dysregulation of adipocytokines, including TNF-α and adiponectin [9–12].

Recently, blockade of the Ang II signal by Ang II type 1 receptor blocker (ARB) was reported to ameliorate insulin sensitivity in experimental animals and hypertensive patients [13–15], thereby possibly suppressing TNF-α production by skeletal muscle. Also, ARB can ameliorate insulin resistance in patients with essential hypertension by increasing the level of serum adiponectin [16]. On the other hand, large-scale randomized control studies have shown that ARB can prevent the development of diabetes mellitus in patients with essential hypertension [17–19].

Hepatic steatosis is associated with visceral obesity and insulin resistance, and may progress to nonalcoholic steatohepatitis (NASH) under certain circumstances. A low level of serum adiponectin and decreased sensitivity to

Published online: 14 April 2009

leptin are common in hepatic steatosis and NASH. Recently, it was reported that ARB is able to suppress hepatic fibrosis by suppressing the activation of stellate cells, which play a major role in production of the extracellular matrix [20]. However, little is known about how Ang II participates in insulin resistance and hepatic steatosis and how ARB is able to ameliorate these conditions.

Stearoyl-CoA desaturase-1 (SCD-1) is an enzyme that desaturates palmitate, the saturated end-product of de novo fatty acid synthesis. SCD-1 expression and monounsaturated fatty acid levels are markedly increased in livers of leptin-deficient *ob/ob* mice [21] and leptin receptor-deficient (*fa/fa*) Zucker diabetic fatty (ZDF) rats [22]. Leptin treatment reduces expression of the SCD-1 gene in these animals, indicating that it has a regulatory role in SCD-1 gene expression. While elucidation of leptin's role has permitted a detailed view of the biology underlying energy homeostasis, most obese individuals are leptin-resistant [23]. The *ob/ob* mice lacking SCD-1 are significantly less obese than *ob/ob* controls and have histologically normal liver with a significant reduction of both triglyceride (TG) storage and production of very low density lipoprotein (VLDL) [21]. Pharmacologic manipulation of SCD-1 may be of benefit in the treatment of obesity, diabetes, hepatic steatosis, and other components of metabolic syndrome. However, no study has yet investigated whether Ang II can regulate SCD-1 gene expression.

In this study, we investigated whether a potent ARB, olmesartan, is able to ameliorate hepatic steatosis and insulin resistance in obese *fa/fa* Zucker rats, which have a defect in the leptin receptor, fed a high-fat diet, and whether expression of the SCD-1 gene in the liver is affected by olmesartan. The SCD-1 gene was found to be overexpressed in the liver of obese rats fed a high-fat diet relative to the level in obese rats fed a standard diet and showed reduced expression following exposure to olmesartan for 4 weeks.

Materials and methods

Animals

Five-week-old male obese (*fa/fa*) Zucker rats were purchased from Charles River Laboratories Japan Inc. (Kanagawa, Japan). All rats were housed in a temperature-controlled room (20–23°C) with a 12-h light/dark cycle (light on 0600–1800 hours), and had free access to a laboratory standard diet and water. All animal studies were done according to a protocol approved by the Animal Experimentation Committee of Yamagata University Faculty of Medicine, Japan.

Experimental design

At 6 weeks of age, the rats were divided into two groups: obese rats fed a standard diet ($n = 5$) and obese rats fed a high-fat diet ($n = 15$). These diets had the following compositions (as a percentage of total calories): standard diet (CRF-1, Charles River Laboratories Japan Inc., 10% fat, 20% protein, and 70% carbohydrate); high-fat diet [no. D12450B, Research Diets Inc., New Brunswick, NJ, 45% fat (predominantly from lard), 20% protein, and 35% carbohydrate]. All animals were fed standard or high-fat diets for 8 weeks until the end of the experiment. After 4 weeks on the diets, the high-fat diet-fed obese rats ($n = 15$) were further divided into three experimental groups ($n = 5$ rats per group) treated with olmesartan at 1 or 10 mg/kg body/day and treated with vehicle (0.5% carboxymethyl cellulose) alone as the control. Olmesartan (CS-866), a potent ARB, was kindly provided by Daiichi-Sankyo Co. Ltd. (Tokyo, Japan). Standard diet-fed obese rats ($n = 5$ rats per group) were treated with vehicle alone. The drug was administered once daily by oral gavage for 4 weeks.

Blood and liver tissue sampling

After the end of drug treatment, all 14-week-old rats were fasted overnight (13–15 h, food removed at 1800 h) and then killed under ether anesthesia. Blood was rapidly collected from the inferior vena cava, and serum was prepared by centrifugation (3,000 rpm, 10 min, 4°C) of the blood and stored at −20°C until further analysis. The liver tissue was immediately removed and snap-frozen in liquid nitrogen, and stored at −80°C until further study.

Biochemical assay of serum components

Serum glucose (Glu), triglyceride (TG), and free fatty acid (FFA) were measured using enzymatic assay kits (Shino-Test Co., Tokyo; Wako Pure Chemical Industries Ltd., Osaka; Eiken Chemical Co. Ltd., Tokyo, Japan, respectively) on a Hitachi Autoanalyzer 7181 (Hitachi High-Technologies Inc., Tokyo, Japan). Serum levels of insulin and adiponectin were respectively measured using a rat insulin ELISA kit (Shibayagi Co. Ltd., Gunma, Japan) and a rat adiponectin ELISA kit (Otsuka Pharmaceutical Co. Ltd., Tokushima, Japan).

Measurement of triglyceride in liver

Lipid extraction was performed by a modified version of the method described previously by Folch [24]. Liver tissues were homogenized with methanol/chloroform (1/2 v/v, 20 ml/g tissue), and aliquots of the organic phase were evaporated under nitrogen gas. The dried lipid extracts

were dissolved in isopropyl alcohol. TG content within the lipid extracts was measured using an enzymatic assay kit (Wako Pure Chemical Industries) on a Hitachi Autoanalyzer 7181 (Hitachi High-Technologies).

Analysis of liver fatty acid

The procedure used for lipid extraction was the same as that for liver TG measurement [24]. Fatty acids in lipids were analyzed using a modification of the method described previously [25]. The dried lipid extracts were treated with 5% KOH–ethanol/water (9/1 v/v) solution. The hydrolyzed lipids were then mixed with *n*-hexane and water, and extracted into the aqueous phase. Pentadecane acid as an internal control was then added to the aqueous phase. The aqueous phase was homogenized with 6 M HCl and *n*-hexane, and the fatty acids were extracted into *n*-hexane, then dried under nitrogen gas and transmethylated with BF_3–methanol/benzene/methanol (7/6/7 v/v/v) solvent at 100°C. Fatty acid methyl esters were extracted into *n*-pentane and analyzed on a gas chromatograph (HP6890 series; Agilent Technologies Japan Ltd., Tokyo, Japan) equipped with a capillary column (DB-WAX; 30 m × 0.32 mm, 0.25 μm film, Agilent Technologies, Japan). Fatty acid methyl esters were identified by comparison with the internal control. SCD-1 activity index was calculated from the precursor-to-product ratio as stearic acid to oleic acid (C18:0/C18:1).

Expression analysis of SCD-1 mRNA in liver

Liver mRNA levels of SCD-1 were measured by real-time PCR with glyceraldehyde-3-phosphate dehydrogenase (GAPDH) as an internal control. Two-step real-time PCR was performed as described previously [26, 27]. Total RNAs were isolated from liver tissues using an RNeasy Plus Mini Kit (QIAGEN Inc., Hilden, Germany). A cDNA was synthesized from 1 μg of total RNA using a random primer (Takara Bio Inc., Mie, Japan) and SuperScript® II RNase H^- Reverse Transcriptase (Invitrogen) in accordance with the manufacturer's instructions. Real-time PCR reactions were performed using a Fast Start DNA Master SYBR I Kit (Roche Diagnostic AG, Basel, Switzerland) on a LightCycler® 2.0 System (Roche Diagnostic). Specific primers were designed using a Perfect Real Time Support System (Takara Bio) and were as follows: SCD-1 (NM1 39192), GCTTGTGGAGCCACAGGACTTAC (forward), ATCCCGGGCCCATTCATATAC (reverse); GAPDH (NM017008), GACAACTTTGGCATCGTGGA (forward), ATGCAGGGATGATGTTCTGG (reverse). PCR reactions for all samples were run in triplicate. Data were analyzed using the LightCycler Software program version 3.5 (Roche Diagnostic). The amounts of all mRNAs were calculated using a standard curve constructed using serial dilutions of a concentrated cDNA sample. The expression level of SCD-1 was normalized with that of GAPDH.

Data analysis and statistics

All data in figures are expressed as mean ± standard error of the mean (SEM). For comparisons between two groups, statistical analysis was performed using unpaired Student's or Welch's *t* test. Mann–Whitney *U* test was used when appropriate. For comparisons among three groups, data were analyzed by one-way ANOVA with the Tukey–Kramer multiple comparisons test. Differences were considered significant at $P < 0.05$.

Results

Amelioration of hyperglycemia, hyperinsulinemia, and insulin resistance by ARB administration

Obese *fa/fa* Zucker rats fed a high-fat diet showed severe hyperglycemia and hyperinsulinemia. Administration of olmesartan at a dose of 10 mg/kg/day for 4 weeks ameliorated the hyperglycemia and hyperinsulinemia in comparison with vehicle treatment in obese rats fed a high-fat diet (glucose: 291.0 ± 20.6 vs. 434.8 ± 52.2 mg/dl, $P < 0.05$; insulin: 29.0 ± 5.3 vs. 49.0 ± 5.6 ng/ml, $P < 0.05$; Fig. 1a, b). These data suggested that ARB is able to ameliorate insulin resistance in obese Zucker rats fed a high-fat diet. The serum concentrations of glucose and insulin in vehicle-treated obese Zucker rats fed a standard diet were 283.8 ± 19.4 mg/dl and 21.3 ± 4.1 ng/ml, respectively.

Decrease in serum FFA level, serum TG level, and hepatic TG content by ARB administration

Olmesartan administration at a dose of 10 mg/kg/day decreased the serum level of FFA in comparison with vehicle treatment in obese rats fed a high-fat diet (697.2 ± 47.5 vs. 1,004.0 ± 215.4 μEQ/l; Fig. 2a), although the difference was not statistically significant. On the other hand, olmesartan administration did not change the serum level of TG (vehicle: 154.6 ± 16.0 vs. olmesartan: 189.6 ± 28.3 and 213.4 ± 31.7 mg/dl; Fig. 2b). Histologically, the hepatocytes of obese rats fed a high-fat diet contained fat droplets in three zones of all hepatic lobules (data not shown). The hepatic TG content was decreased dose-dependently by olmesartan administration at 1 and 10 mg/kg/day (vehicle: 362.9 ± 27.8 vs. olmesartan: 252.8 ± 25.3 and 215.1 ± 21.2 mg/g liver, $P < 0.05$ and $P < 0.005$, respectively; Fig. 2c), suggesting that ARB worked to ameliorate fatty

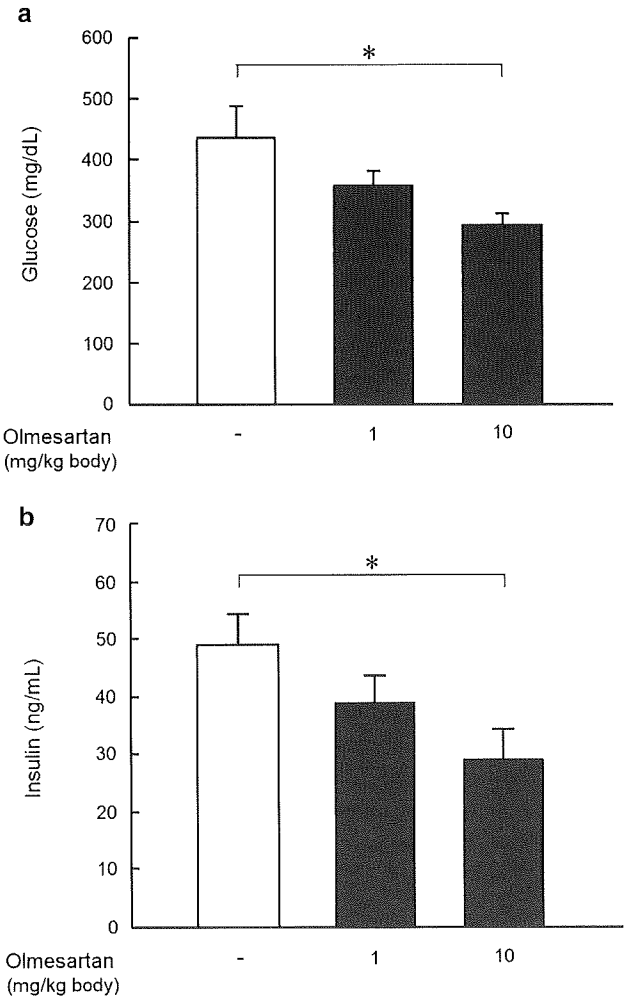

Fig. 1 Effect of olmesartan on serum levels of glucose and insulin in obese Zucker rats fed a high-fat diet. Serum levels of (**a**) glucose and (**b**) insulin in high-fat diet-fed obese Zucker rats treated with olmesartan (1 or 10 mg/kg body/day) for 4 weeks and treated with vehicle alone as the control. High-fat diet was fed to rats for 8 weeks from 6 to 14 weeks of age. Values are mean ± SEM ($n = 5$) for these separate experiments. *$P < 0.05$

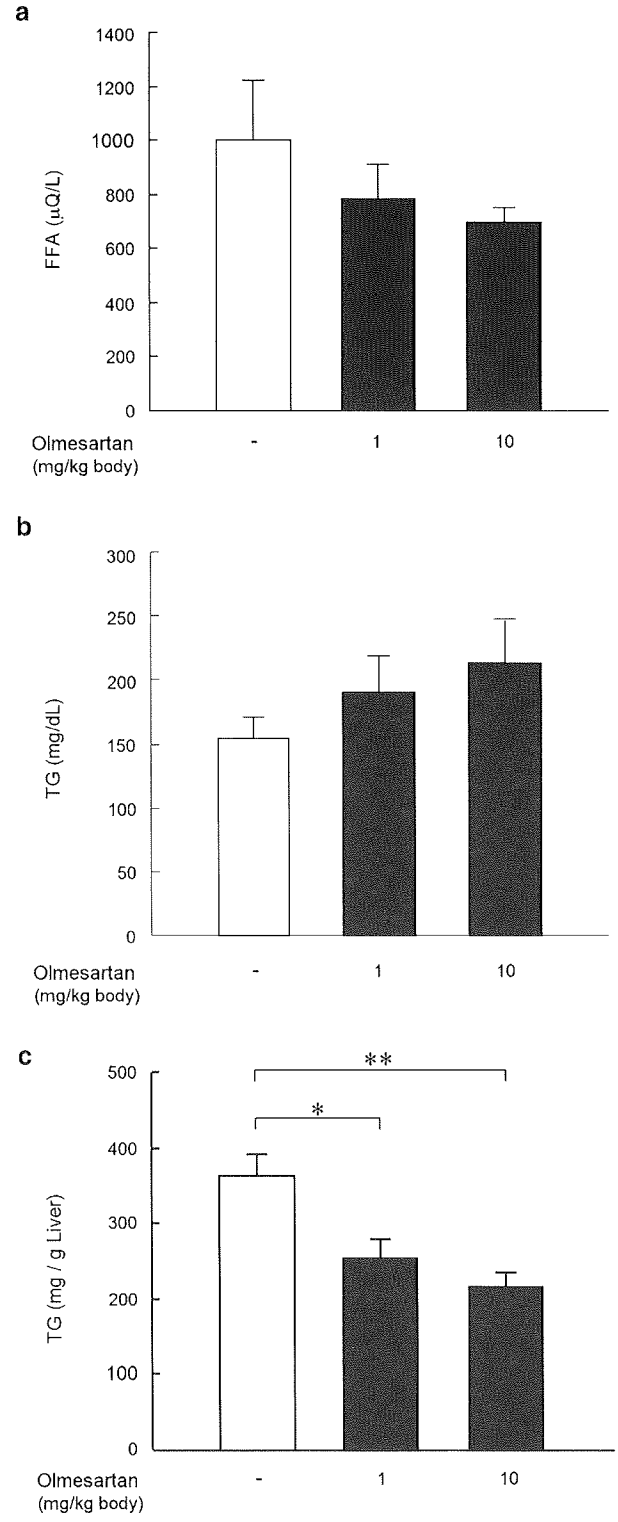

Fig. 2 Effect of olmesartan on serum triglyceride, serum free fatty acid, and liver triglyceride in obese Zucker rats fed a high-fat diet. (**a**) Serum free fatty acid (FFA) level and triglyceride (TG) level in serum (**b**) and liver (**c**) are shown, respectively, in groups of high-fat diet-fed obese rats treated with olmesartan (1 or 10 mg/kg body/day) for 4 weeks and treated with vehicle alone as the control. High-fat diet was fed to rats for 8 weeks from 6 to 14 weeks of age. Values are mean ± SEM ($n = 5$) for these separate experiments. *$P < 0.05$, **$P < 0.01$

liver in obese rats fed a high-fat diet. The serum concentrations of FFA and TG, and the hepatic TG content in obese Zucker rats fed a standard diet were 650.4 ± 80.7 μEQ/l, 554.2 ± 43.8 mg/dl, and 95.1 ± 15.9 mg/g liver, respectively.

Increase of serum adiponectin level by ARB administration

Olmesartan administration at a dose of 10 mg/kg/day increased the serum adiponectin level in comparison with vehicle treatment in obese rats fed a high-fat diet (8.2 ± 0.9 vs. 5.1 ± 0.5 μg/ml, $P < 0.05$; Fig. 3), suggesting a mechanism for improvement of glucose and fat

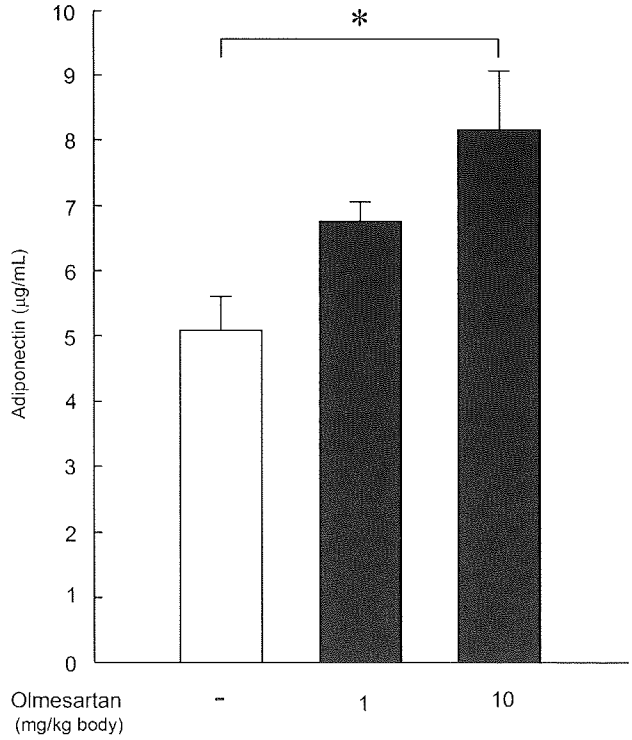

Fig. 3 Effect of olmesartan on serum adiponectin levels in obese Zucker rats fed a high-fat diet. Serum adiponectin levels are shown in groups of high-fat diet-fed obese rats treated with olmesartan (1 or 10 mg/kg body/day) for 4 weeks and treated with vehicle alone as the control. High-fat diet was fed to rats for 8 weeks from 6 to 14 weeks of age. Values are mean ± SEM ($n = 5$) for these separate experiments. *$P < 0.05$

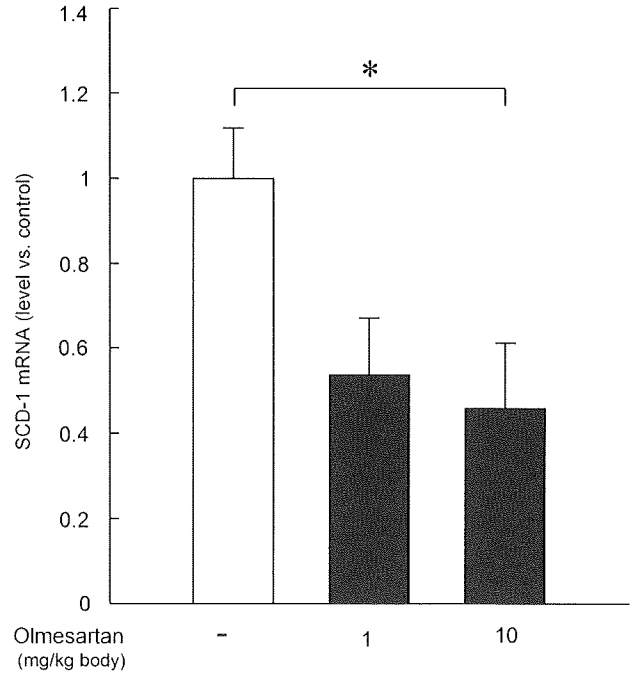

Fig. 4 Effect of olmesartan on SCD-1 mRNA level in liver of obese Zucker rats fed a high-fat diet. Expression levels of SCD-1 in liver were determined by real-time PCR and expressed as a ratio relative to that of GAPDH mRNA as an internal control. Comparisons of SCD-1 mRNA expression in liver samples are shown for groups of high-fat diet-fed obese Zucker rats treated with olmesartan (1 or 10 mg/kg body/day) for 4 weeks and treated with vehicle alone as the control. A high-fat diet was fed to rats for 8 weeks from 6 to 14 weeks of age. Values are mean ± SEM ($n = 5$) for these separate experiments, and that for a vehicle-treated control obese rat is set as 1.0. *$P < 0.05$

metabolism. The serum adiponectin level in obese Zucker rats fed a standard diet was 7.9 ± 0.6 ng/ml.

Down-regulation of SCD-1 gene expression by ARB administration

All data were expressed as the SCD-1/GAPDH mRNA ratio in the same samples taken from obese Zucker rats fed a high-fat diet, and that of vehicle-treated control obese rats was set as 1.00 (Fig. 4). Olmesartan administration at a dose of 10 mg/kg/day decreased the level of SCD-1 mRNA by 46% compared with that observed in the vehicle-treated control rats fed a high-fat diet (1.00 ± 0.12 vs. 0.46 ± 0.15, $P < 0.05$; Fig. 4). The level of SCD-1 mRNA in obese Zucker rats fed a standard diet was 0.55 ± 0.09.

To confirm the decrease of SCD-1 gene expression induced by ARB in vivo, we examined the ratio of stearic acid (C18:0) to oleic acid (C18:1) in the liver of obese Zucker rats fed a high-fat diet. The ratio in vehicle-treated control obese rats was set as 1.0 (Fig. 5). Olmesartan administration at a dose of 10 mg/kg/day increased the ratio 1.4-fold relative to that observed in vehicle-treated control rats fed a high-fat diet ($P < 0.01$, Fig. 5), suggesting a decrease of SCD-1 activity in the liver. The ratio of C18:0 to C18:1 in the liver of obese Zucker rats fed a standard diet was 2.64 ± 0.39.

Discussion

Obese *fa/fa* Zucker rats fed a high-fat diet showed more severe hepatic steatosis and insulin resistance than obese rats fed a standard diet, suggesting that obese rats fed a high-fat diet are a good model for examining whether ARB administration can ameliorate hepatic steatosis and insulin resistance. In this study, olmesartan, a potent ARB, markedly decreased fasting blood levels of glucose and insulin, as well as the hepatic TG content, in obese Zucker rats fed a high-fat diet. These observations are also consistent with a previous study [28] of obese Zucker rats fed a standard diet. Our present data indicate that olmesartan ameliorates insulin resistance and hepatic steatosis, suggesting that the Ang II signal induces insulin resistance and hepatic steatosis, as described previously for other ARB agents [13–15].

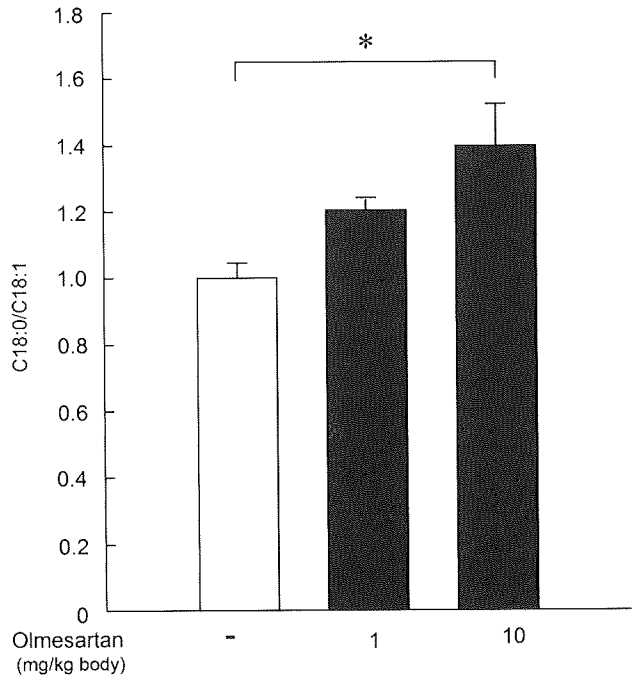

Fig. 5 Effect of olmesartan on fatty acid desaturation in liver of obese Zucker rats fed a high-fat diet. Values are expressed as the ratio of the levels of stearic acid (C18:0, saturated fatty acid) to oleic acid (C18:1, monounsaturated fatty acid) in liver. Comparisons of fatty acid ratio are shown in groups of high-fat diet-fed obese rats treated with olmesartan (1 or 10 mg/kg body/day) for 4 weeks and treated with vehicle alone as the control. High-fat diet was fed to rats for 8 weeks from 6 to 14 weeks of age. Values are mean ± SEM ($n = 5$) for these separate experiments, and that for a standard diet-fed obese rats is set as 1.0. $*P < 0.05$

Indeed, it is known that Ang II stimulates serine-phosphorylation of the insulin receptor, insulin receptor substrate 1 (IRS-1), and phosphatidylinositol (PI) 3-kinase via the angiotensin II type 1 (AT1) receptor in insulin signal transduction [10]. As a result, the inhibition of insulin signaling induces insulin resistance. Therefore, our data suggest that inhibition of Ang II signaling via the AT1 receptor by ARB results in recovery of insulin signal transduction, thereby ameliorating insulin resistance.

Adiponectin, a hormone secreted by adipocytes, acts as a major antidiabetic and atherogenic adipocytokine [29]. Plasma adiponectin levels are decreased in obesity, insulin resistance, and type 2 diabetes [29]. Decreased adiponectin is implicated in the development of insulin resistance in obesity, which is reversed by replenishment of adiponectin [30–32]. This insulin-sensitizing effect of adiponectin seems to be mediated by inhibition of gluconeogenesis and stimulation of fatty acid oxidation via activation of AMP-activated protein kinase (AMPK) and peroxisome proliferator-activated receptor (PPAR)-α [33–35]. In this study, olmesartan administration increased the serum level of adiponectin, an action that could partly explain the amelioration of insulin resistance [16].

To investigate whether SCD-1 gene expression is affected by ARB via blockade of the AT1 receptor signal, we used a real-time PCR assay. We noticed that expression of the SCD-1 gene was significantly increased in the liver of obese rats fed a high-fat diet in comparison with that in the liver of obese rats fed a standard diet. Real-time PCR demonstrated that after olmesartan administration for 4 weeks at a dose of 10 mg/kg body/day, SCD-1 gene expression in obese rats fed a high-fat diet was restored to the level observed in obese rats fed a standard diet.

SCD-1 is the rate-limiting enzyme in the biosynthesis of monounsaturated fatty acids, introducing a single double bond into its substrates, palmitic (16:0) and stearic (18:0) acids, to generate palmitoleic (16:1) and oleic (18:1) acids as products [36, 37]. The enzyme is located predominantly in the endoplasmic reticulum, where it undergoes rapid turnover in response to a variety of nutritional and hormonal signals [38]. The gene is also transcriptionally regulated by a number of factors including sterol regulatory element-binding protein 1 (SREBP-1) and polyunsaturated fatty acid (PUFA) [39, 40].

Regulation of SCD-1 by leptin seems to be relatively specific [22], although the precise mechanism by which the hormone represses the enzyme is currently unknown. Recent studies of SCD-1 have yielded many new insights into the biology of lipid metabolism and have demonstrated that mice lacking SCD-1 (SCD-$1^{-/-}$ mice) are resistant to high-fat diet-induced obesity and glucose intolerance [41]. A consequence of SCD-1 deficiency is activation of lipid oxidation in addition to reduced TG synthesis and storage. Furthermore, SCD-$1^{-/-}$ mice exhibit increased thermogenesis and insulin signaling in skeletal muscle and brown adipose tissue [42–44]. These lines of evidence have revealed that SCD-1 is an important metabolic control point in lipid metabolism and a promising drug target for the treatment of metabolic syndrome.

In vivo antisense oligonucleotide (ASO) reduction of target genes is a powerful tool for identifying novel metabolic drug targets and elucidating the role of various genes in cellular metabolic pathways. Two recent studies have shown that an ASO-mediated approach can prevent the development of high-fat diet-induced obesity, hepatic steatosis, and insulin resistance [45, 46]. To examine whether SCD-1 activity is inhibited by olmesartan in vivo, we analyzed the ratio of stearic acid (C18:0) to oleic acid (C18:1) in the liver of obese Zucker rats fed a high-fat diet. The ratio was significantly increased by olmesartan, suggesting that SCD-1 activity was suppressed in the liver.

This study showed that ARB can improve insulin resistance and hepatic steatosis in obese rats fed a high-fat diet. This improvement may be partly explained by an increase of adiponectin, as reported previously [33–35]. In

addition, the present data suggest that the ARB-induced decrease of SCD-1 gene expression in the liver participates in the improvement of insulin resistance and hepatic steatosis independently of leptin signaling. However, it is still unknown whether changes in SCD-1 occur as a direct result of ARB on liver cells or as a consequence of systemic changes or changes in body composition, and whether SCD-1 is a direct target of Ang II or the AT1 receptor.

In addition, it has recently been reported that ARB can reduce SREBP-1c gene expression [47]. Accordingly, it would also be expected that SCD-1 gene expression may be partly decreased via suppression of SREBP-1 gene expression by ARB. This issue should be clarified by in vitro experiments using primary hepatocytes or hepatoma cells to examine whether they show direct regulation of SCD-1 gene expression by ARB, and this is currently underway in our laboratory. In this study, ARB treatment caused an increase in the serum adiponectin level and suppressed hepatic SCD-1 expression in obese Zucker rat fed a high-fat diet. However, no previous report has indicated that adiponectin is related to the regulation of SCD-1 gene expression. Therefore, further investigation is needed to clarify whether adiponectin signaling suppresses SCD-1 gene expression.

Previous studies demonstrated that Ang II stimulation via the AT1 receptor increases the gene expression and secretion of leptin in human or rat adipocytes [48, 49] and that administration of ARB suppresses leptin production by inhibition of Ang II signaling [50]. In this study we showed that the serum insulin level and hepatic TG content of obese Zucker rats fed a high-fat diet were significantly increased approximately two- and four-fold relative to those fed a standard diet, respectively. Additionally, in lean Zucker rats fed a high-fat diet, the serum insulin level and hepatic TG content were also significantly increased approximately two- and five-fold, respectively (data not shown). After olmesartan administration, the serum insulin level and hepatic TG content of obese Zucker rats fed a high-fat diet were both decreased to 60% of the values in the vehicle-treated control. On the other hand, in lean Zucker rats, the serum insulin level and hepatic TG content were decreased to approximately 40 and 27% (data not shown). These observations suggest that the effects of ARB on insulin resistance and hepatic steatosis were greater in lean Zucker rats than in obese Zucker rats. The differences in efficacy of ARB between these two models may be partly due to the differences in leptin action. In the case of the normal leptin receptor, leptin signaling may also partly contribute to the effects of ARB on insulin resistance and hepatic steatosis, thereby increasing the effects of ARB in comparison with leptin receptor deficiency.

In conclusion, our present study has shown that obese *fa/fa* Zucker rats, which have a deficiency of the leptin receptor, develop serious insulin resistance and hepatic steatosis when fed a high-fat diet. Moreover, the mRNA level of SCD-1, a key enzyme in hepatic lipogenesis, is evidently increased in the liver. A potent ARB, olmesartan, was able to ameliorate insulin resistance and hepatic steatosis and to suppress the gene expression of hepatic SCD-1. These data suggest that olmesartan-induced down-regulation of SCD-1 gene expression is partly involved in the amelioration of insulin resistance and hepatic steatosis.

References

1. Ford ES, Giles WH. A comparison of the prevalence of the metabolic syndrome using two proposed definition. Diabetes Care. 2003;26:575–81.
2. West DB, Boozer CN, Moody DL, Atkinson RL. Dietary obesity in nine inbred mouse strains. Am J Physiol. 1992;262:R1025–32.
3. West DB, Waguespack J, McCollister S. Dietary obesity in the mouse: interaction of strain with diet composition. Am J Physiol. 1995;268:R658–65.
4. Buettner R, Ottinger I, Schölmerich J, Bollheimer LC. Preserved direct hepatic insulin action in rats with diet-induced hepatic steatosis. Am J Physiol Endocrinol Metab. 2004;286:E828–33.
5. Flegal KM, Carroll MD, Ogden CL, Johnson CL. Prevalence and trends in obesity among US adults, 1999–2000. JAMA. 2002;288:1723–7.
6. Friedman JM. Obesity in the new millennium. Nature. 2000; 404:632–4.
7. Karlsson C, Lidell K, Ottosson M, Sjostrom L, Carlsson B, Carlsson LM. Human adipose tissue expresses angiotensinogen and enzymes required for its conversion to angiotensin II. J Clin Endocrinol Metab. 1998;83:3925–9.
8. Matsushita K, Wu Y, Okamoto Y, Pratt RE, Dzau VJ. Local renin–angiotensin expression regulates human mesenchymal stem cell differentiation to adipocytes. Hypertension. 2006;48: 1095–102.
9. Richey JM, Ader M, Moore D, Bergman RN. Angiotensin II induces insulin resistance independent of changes in interstitial insulin. Am J Physiol. 1999;277:E920–6.
10. Folli F, Kahn CR, Hansen H, Bouchie JL, Feener EP. Angiotensin II inhibits insulin signal in aortic smooth muscle cells at multiple levels. A potential role for serine phosphorylation in insulin/angiotensin II crosstalk. J Clin Invest. 1997;100:2158–69.
11. Togashi N, Ura N, Higashiura K, Murakami H, Shimamoto K. The contribution of skeletal muscle tumor necrosis factor-alpha to insulin resistance and hypertension in fructose-fed rats. J Hypertens. 2000;18:1605–10.
12. Maeda N, Shimomura I, Kishida K, Nishizawa H, Matsuda M, Nagaretani H, et al. Diet-induced insulin resistance in mice lacking adiponectin/ACRP30. Nature Med. 2002;8:731–7.
13. Iimura O, Shimamoto K, Matsuda K, Masuda A, Takizawa H, Higashiura K, et al. Effects of angiotensin receptor antagonist and angiotensin converting enzyme inhibitor on insulin sensitivity in fructose-fed hypertensive rats and essential hypertensives. Am J Hypertens. 1994;8:450–5.
14. Navarro-Cid J, Maeso R, Perez-Vizcaino F, Cachofeiro V, Ruilope LM, Tamargo J, et al. Effects of losartan on blood pressure,

metabolic alterations, and vascular reactivity in the fructose-induced hypertensive rat. Hypertension. 1995;26:1074–8.
15. Higashiura K, Ura N, Takada T, Agata J, Yoshida H, Miyazaki Y, et al. Alteration of muscle fiber composition linking to insulin resistance and hypertension in fructose-fed rats. Am J Hypertens. 1999;12:596–602.
16. Furuhashi M, Ura N, Higashiura K, Murakami H, Tanaka M, Moniwa N, et al. Blockade of the renin–angiotensin system increases adiponectin concentrations in patients with essential hypertension. Hypertension. 2003;42:76–81.
17. Lithell H, Hansson L, Skoog I, Elmfeldt D, Hofman A, Olofsson B, et al. The study on cognition and prognosis in the elderly (SCOPE): principal results of a randomized double-blind intervention trial. J Hypertens. 2003;21:875–86.
18. Dahlof B, Devereux RB, Kjeldsen SE, Julius S, Beevers G, de Faire U, et al. Cardiovascular morbidity and mortality in the Losartan intervention for endpoint reduction in hypertension study (LIFE): a randomised trial against atenolol. Lancet. 2002; 359:995–1003.
19. Julius S, Kjeldsen SE, Weber M, Brunner HR, Ekman S, Hansson L, et al. Outcomes in hypertensive patients at high cardiovascular risk treated with regimens based on valsartan or amlodipine: the VALUE randomised trial. Lancet. 2004;363:2022–31.
20. Yokohama S, Yoneda M, Haneda M, Okamoto S, Okada M, Aso K, et al. Therapeutic efficacy of an angiotensin II receptor antagonist in patients with nonalcoholic steatohepatitis. Hepatology. 2004;40:1222–5.
21. Cohen P, Miyazaki M, Socci ND, Hagge-Greenberg A, Liedtke W, Soukas AA, et al. Role for stearoyl-CoA desaturase-1 in leptin-mediated weight loss. Science. 2002;297:240–3.
22. Kakuma T, Lee Y, Unger RH. Effects of leptin, troglitazone, and dietary fat on stearoyl CoA desaturase. Biochem Biophys Res Commun. 2002;297:1259–63.
23. Cohen P, Ntambi JM, Friedman JM. Stearoyl-CoA desaturase-1 and the metabolic syndrome. Curr Drug Targets Immune Endocr Metabol Disord. 2003;3:271–80.
24. Folch J, Lees M, Sloane SGH. A simple method for the isolation and purification of total lipids from animal tissues. J Biol Chem. 1957;226:497–509.
25. Archibald FM, Skipski VP. Determination of fatty acid content and composition in ultramicro lipid samples by gas–liquid chromatography. J Lipid Res. 1966;7:442–5.
26. Komamura K, Shirotani-Ikejima H, Tatsumi R, Tsujita-Kuroda Y, Kitakaze M, Miyatake K, et al. Differential gene expression in the rat skeletal and heart muscle in glucocorticoid-induced myopathy: analysis by microarray. Cardiovasc Drugs Ther. 2003;17:303–10.
27. Miyazaki M, Gomez FE, Ntambi JM. Lack of stearoyl-CoA desaturase-1 function induces a palmitoyl-CoA Delta6 desaturase and represses the stearoyl-CoA desaturase-3 gene in the preputial glands of the mouse. J Lipid Res. 2002;43:2146–54.
28. Ran J, Hirano T, Adachi M. Angiotensin II type 1 receptor blocker ameliorates overproduction and accumulation of triglyceride in the liver of Zucker fatty rats. Am J Physiol Endocrinol Metab. 2004;287:E227–32.
29. Matsuzawa Y. The metabolic syndrome and adipocytokines. FEBS Lett. 2006;580:2917–21.
30. Fruebis J, Tsao TS, Javorschi S, Ebbets-Reed D, Erickson MR, Yen FT, et al. Proteolytic cleavage product of 30-kDa adipocyte complement-related protein increases fatty acid oxidation in muscle and causes weight loss in mice. Proc Natl Acad Sci USA. 2001;98:2005–10.
31. Yamauchi T, Kamon J, Waki H, Terauchi Y, Kubota N, Hara K, et al. The fat-derived hormone adiponectin reverses insulin resistance associated with both lipoatrophy and obesity. Nat Med. 2001;7:941–6.
32. Berg AH, Combs TP, Du X, Brownlee M, Scherer PE. The adipocyte-secreted protein Acrp30 enhances hepatic insulin action. Nat Med. 2001;7:947–53.
33. Yamauchi T, Kamon J, Minokoshi Y, Ito Y, Waki H, Uchida S, et al. Adiponectin stimulates glucose utilization and fatty-acid oxidation by activating AMP-activated protein kinase. Nat Med. 2002;8:1288–95.
34. Tomas E, Tsao TS, Saha AK, Murrey HE, Zhang Cc C, Itani SI, et al. Enhanced muscle fat oxidation and glucose transport by ACRP30 globular domain: acetyl-CoA carboxylase inhibition and AMP-activated protein kinase activation. Proc Natl Acad Sci USA. 2002;99:16309–13.
35. Kersten S, Desvergne B, Wahli W. Roles of PPARs in health and disease. Nature. 2000;405:421–4.
36. Ntambi JM, Buhrow SA, Kaestner KH, Christy RJ, Sibley E, Kelly TJ Jr, et al. Differentiation-induced gene expression in 3T3–L1 preadipocytes. Characterization of a differentially expressed gene encoding stearoyl-CoA desaturase. J Biol Chem. 1988;263:17291–300.
37. Miyazaki M, Ntambi JM. Role of stearoyl-coenzyme A desaturase in lipid metabolism. Prostaglandins Leukot Essent Fatty Acids. 2003;68:113–21.
38. Heinemann FS, Ozols J. Stearoyl-CoA desaturase, a short-lived protein of endoplasmic reticulum with multiple control mechanisms. Prostaglandins Leukot Essent Fatty Acids. 2003;68: 123–33.
39. Ntambi JM, Bene H. Polyunsaturated fatty acid regulation of gene expression. J Mol Neurosci. 2001;16:273–8.
40. Zheng Y, Prouty SM, Harmon A, Sundberg JP, Stenn KS, Parimoo S. Scd3—a novel gene of the stearoyl-CoA desaturase family with restricted expression in skin. Genomics. 2001;71: 182–91.
41. Ntambi JM, Miyazaki M, Stoehr JP, Lan H, Kendziorski CM, Yandell BS, et al. Loss of stearoyl-CoA desaturase-1 function protects mice against adiposity. Proc Natl Acad Sci USA. 2002;99:11482–6.
42. Rahman SM, Dobrzyn A, Dobrzyn P, Lee SH, Miyazaki M, Ntambi JM. Stearoyl-CoA desaturase 1 deficiency elevates insulin-signaling components and down-regulates protein-tyrosine phosphatase 1B in muscle. Proc Natl Acad Sci USA. 2003; 100:11110–5.
43. Lee SH, Dobrzyn A, Dobrzyn P, Rahman SM, Miyazaki M, Ntambi JM. Lack of stearoyl-CoA desaturase 1 upregulates basal thermogenesis but causes hypothermia in a cold environment. J Lipid Res. 2004;45:1674–82.
44. Rahman SM, Dobrzyn A, Lee SH, Dobrzyn P, Miyazaki M, Ntambi JM. Stearoyl-CoA desaturase 1 deficiency increases insulin signaling and glycogen accumulation in brown adipose tissue. Am J Physiol Endocrinol Metab. 2005;288: E381–7.
45. Jiang G, Li Z, Liu F, Ellsworth K, Dallas-Yang Q, Wu M, et al. Prevention of obesity in mice by antisense oligonucleotide inhibitors of stearoyl-CoA desaturase-1. J Clin Invest. 2005;115: 1030–8.
46. Gutierrez-Juarez R, Pocai A, Mulas C, Ono H, Bhanot S, Monia BP, et al. Critical role of stearoyl-CoA desaturase-1 (SCD1) in the onset of diet-induced hepatic insulin resistance. J Clin Invest. 2006;116:1686–95.
47. Kurita S, Takamura T, Ota T, Matsuzawa-Nagata N, Kita Y, Uno M, et al. Olmesartan ameliorates a dietary rat model of nonalcoholic steatohepatitis through its pleiotropic effects. Eur J Pharmacol. 2008;588:316–24.
48. Kim S, Whelan J, Claycombe K, Reath DB, Moustaid-Moussa N. Angiotensin II increases leptin secretion by 3T3–L1 and human adipocytes via a prostaglandin-independent mechanism. J Nutr. 2002;132:1135–40.

49. Cassis LA, English VL, Bharadwaj K, Boustany CM. Differential effects of local versus systemic angiotensin II in the regulation of leptin release from adipocytes. Endocrinology. 2004;145:169–74.
50. Zorad S, Dou JT, Benicky J, Hutanu D, Tybitanclova K, Zhou J, et al. Long-term angiotensin II AT1 receptor inhibition produces adipose tissue hypotrophy accompanied by increased expression of adiponectin and PPARgamma. Eur J Pharmacol. 2006;552: 112–22.